

Finite-Time Model-Learning Based \mathcal{L}_1 -Simplex For Integrated TCS and ABS

Yanbing Mao, Naira Hovakimyan, Petros Voulgaris, and Lui Sha

Abstract—This paper proposes an \mathcal{L}_1 -Simplex architecture with finite-time model learning to address safe autonomous velocity regulation for vehicles driving in dynamic and unforeseen environments. To guarantee the reliability of autonomous vehicles, an \mathcal{L}_1 adaptive controller, which compensates for uncertainties and disturbances, is employed by the Simplex architecture as a verified safe controller to tolerate concurrent software and physical failures. Meanwhile, safe switching controller is incorporated into Simplex to achieve the safe velocity tracking through integration of the traction control system (TCS) and anti-lock braking system (ABS). Specifically, the vehicle's velocity asymptotically tracks its provided references that vary with driving environments, while restricts its wheel slip to safe sets to prevent slipping and sliding. Due to the high dependence of the vehicle dynamics on the operational environment, Simplex leverages finite-time model learning to timely learn and update the vehicle model for \mathcal{L}_1 adaptive controller, when any deviation from the safety envelope or the uncertainty measurement threshold occurs in unforeseen driving environments. Simulations demonstrate the effectiveness of the proposed \mathcal{L}_1 -Simplex with model learning in different scenarios.

Index Terms— \mathcal{L}_1 -Simplex, \mathcal{L}_1 adaptive control, finite-time model learning, traction control system, anti-lock braking system.

I. INTRODUCTION

INTELLIGENT transportation systems (ITS) that embed vehicles, roads, traffic lights, message signs, along with microchips and sensors are bringing significant improvements in transportation system performance, including reduced congestion, increased safety and traveler convenience [1]. Intelligent vehicles that aim to improve traffic safety, transport efficiency and driving comfort are playing a major role in ITS, among which the longitudinal vehicle dynamics control is an important aspect. Traction control system (TCS) and anti-lock braking system (ABS) are representative technologies for longitudinal vehicle dynamic control systems [2]. Specifically, ABS is primarily designed to prevent excessive or insufficient wheel slip to keep vehicle steerable and stable during intense braking events, which contributes to high brake performance and road safety [3]–[5], while TCS primarily regulates wheel slip to reduce or eliminate excessive slipping or sliding during vehicle acceleration, which results in better drivability, safety

and traction performance in adverse weather or traffic conditions [6]–[10]. Both TCS and ABS are complicated by nonlinearities, uncertainties and parameter variations, which are induced by variations in the disc-pad friction coefficient [11], nonlinear relation between brake torque and pressure [11], nonlinear wheel-slip characteristics [7], among many others. To regulate slip in these challenging scenarios, various model-based control schemes have been proposed, e.g., proportional-integral-derivative control in combination with sliding mode observer [12], fuzzy control [13], model predictive control [6], sliding mode control [14], H_∞ control [15] and the comparisons therein for an excellent overview.

Autonomous velocity regulation has gained a vital importance [16]–[18], which is motivated by, for example, the imposed speed limits on driving zones (see e.g., school zone and commercial street) and required relative positions with respect to surrounding vehicles and obstacles for safety and transport efficiency. Velocity regulation needs the vehicle to operate in either drive or brake mode. However, it ignores the wheel slip regulation [16]–[18], which has always been a common control objective of TCS and ABS. This implies that simultaneous velocity and slip regulations need the integration of TCS and ABS for enhanced safety, drivability, stability and steerability [3]–[10]. Inspired by these observations, this paper focuses on *safe autonomous velocity regulation*. More concretely, the vehicle asymptotically steers its velocity to the provided references that depend on driving environments, while restricts its wheel slip to safe sets to prevent slipping and sliding during intense braking and accelerating events.

As a typical cyber-physical system, autonomous vehicles integrate the vehicular cyber system with the vehicular physical system for control and operation, whose increasing complexity hinders its reliability, especially when system failures occur. The Simplex architecture provides a reliable control system via software approach, whose core idea is to tolerate some software failures [19]. For the autonomous vehicle, its complicated control missions, see e.g., traction control, lane keeping, collision avoidance, adaptive cruise control and parallel parking, exacerbate the difficulty of keeping the system safe in the presence of physical failures, since the control actuation computed in cyber layer depends on the physical modeling. In addition, the inaccurate vehicle and/or tire parameters are the main obstacles for preventing wheel slip-based control in TCS and ABS. Therefore, the Simplex architecture needs an adaptive controller (which can compensate for model and parameter uncertainties) as a verified safe controller to tolerate physical failures as well. Among the various adaptive control methods, \mathcal{L}_1 adaptive controller has been widely adopted due

Y. Mao and N. Hovakimyan are with the Department of Mechanical Science and Engineering, University of Illinois at Urbana–Champaign, Urbana, IL, 61801 USA (e-mail: {ybm, nhovakim}@illinois.edu).

P. Voulgaris is with the Department of Mechanical Engineering, University of Nevada, Reno, NV, 89557 USA (e-mail: pvoulgaris@unr.edu).

L. Sha is with the Department of Computer Science, University of Illinois at Urbana–Champaign, Urbana, IL, 61801 (e-mail: lrs@cs.uiuc.edu).

This work was supported by NSF (award numbers CMMI-1663460, ECCS-1739732 and CPS-1932529).

to its fast adaptation, guaranteed robustness, and predictable transient response [20], [21]. Considering that \mathcal{L}_1 adaptive control has been verified consistently with the theory in dealing with physical failures with transient performance and robustness guarantees [22]–[24], Wang et al. in [25] proposed a \mathcal{L}_1 -Simplex to address concurrent software and physical failures. Inspired by the attractive properties of \mathcal{L}_1 -Simplex, this paper considers its variant in autonomous vehicles for *safe autonomous velocity regulation*, where \mathcal{L}_1 adaptive control works as a verified safe controller that compensates for uncertainties, disturbances, software and physical failures.

One of the fundamental assumptions of model-based controllers is the availability of a good model of the underlying dynamics in consideration. However, vehicle dynamics highly depend on the driving environments [6], [7], and can be significantly different from one road (e.g., asphalt) to another (e.g., snow). Therefore, a single off-line-built vehicle model cannot capture the dynamics differences induced by environmental variations. To address the model mismatch issue, we bring switching control scheme into \mathcal{L}_1 -Simplex, where multiple normal vehicle models that correspond to different environments (e.g., snow and icy) are stored in \mathcal{L}_1 adaptive control architecture. The objective of switching \mathcal{L}_1 adaptive controller is to achieve safe autonomous velocity regulation in *dynamic normal* driving environments.

Due to the high dependence of vehicle dynamics on driving environments (including air mass density, wind velocity and road friction coefficient, [26]), it is unreasonable to expect that the off-line-built multiple models are sufficient to accurately describe the vehicle-environment interaction dynamics in an unforeseen or unprepared environment, as e.g. the 2019 New York City Snow Squall [27]. If the unforeseen environments cause deviation from the safety envelope or the uncertainty measurement threshold in the time-critical environment, it is necessary to use limited sensor data to timely learn and update the vehicle model for reliable decision making. In recent several years, significant effort has been devoted towards the sample complexity bound of ordinary least-square based finite-time model learning [28]–[32], including lower bounds on model error and the upper bounds on the number of observations sufficient to identify system model with prescribed levels of accuracy and confidence. The sample complexity bounds obtained therein rely on the assumption that the discretization of real systems can be described by $x(k+1) = Ax(k) + f(k+1)$, where $x(k)$ and $f(k)$ denote state observations and random bias, respectively. Even more importantly, the bias process $\{f(k)\}_{k=1}^{\infty}$ drawn independently is assumed to have zero-mean, unit-variance, independent coordinates, which prevents the applications of the obtained results in [28]–[32] to fairly general systems that have dependence structures, i.e., the random vector $f(k)$ has dependencies on time k and/or coordinates. To remove the obstacles that prevent learning dynamical systems with dependence structures, we proposed a novel finite-time model learning with complexity bounds in [33], which will be used to timely learn and update a vehicle model for \mathcal{L}_1 -Simplex in unforeseen driving environments.

To this end, we propose a \mathcal{L}_1 -Simplex architecture with safe switching control and finite-time model learning for

autonomous vehicles, which is able to achieve

- safe autonomous velocity regulation in dynamic and unforeseen driving environments;
- tolerance of concurrent software and physical failures.

This paper is organized as follows. In Section II, we present the preliminaries including longitudinal vehicle model and model-learning based \mathcal{L}_1 -Simplex architecture. Safety envelope is formulated in Section III. In Section IV, we present the off-line-built ideal vehicle model and finite-time model learning procedure. We investigate the safe switching control of off-line-built models and inferred model via model learning in Section V, building on which Section VI presents \mathcal{L}_1 -Simplex design. We present numerical simulations in Section VII. We finally present our conclusions and future research directions in Section VIII.

II. PRELIMINARIES

A. Notation

We let \mathbb{R}^2 denote the set of two dimensional real vectors. $\mathbb{R}^{2 \times 2}$ denotes the set of 2×2 -dimensional real matrices. \mathbb{N} stands for the set of natural numbers, and $\mathbb{N}_0 = \mathbb{N} \cup \{0\}$. $\mathbb{V} \setminus \mathbb{K}$ stands for the complement set of \mathbb{K} with respect to \mathbb{V} . \mathbf{I} and $\mathbf{1}$, respectively, denote the identity matrix and vectors of all ones with proper dimensions. For $x \in \mathbb{R}^2$, $\|x\| = \sqrt{x_1^2 + x_2^2}$. For $A \in \mathbb{R}^{2 \times 2}$, $\|A\|$ denotes the induced 2-norm of a matrix A . The superscript ‘ \top ’ stands for matrix transpose. We use $P > (<) 0$ to denote a positive definite (negative definite) matrix P . Given a symmetric matrix P , $\lambda_{\min}(P)$ and $\lambda_{\max}(P)$ are the minimum and maximum eigenvalues, respectively. \mathcal{L}_1 norm of a function $x(t)$ is denoted by $\|x(t)\|_{\mathcal{L}_1}$, and $\|x\|_{\mathcal{L}_\infty[a,b]} = \sup_{a \leq t \leq b} \|x(t)\|$. We denote $x(s) = \mathfrak{L}\{x(t)\}$, where $\mathfrak{L}(\cdot)$ stands for the Laplace transform operator. The gradient of $f(x)$ at x is denoted by $\nabla f(x)$. The parameter notations of vehicle model are given in Table I.

Table I
VEHICLE MODEL PARAMETERS

w	Angular velocity
v	Longitudinal velocity
J	Wheel rotational inertia
T_b	Brake torque
T_c	Friction torque on wheel
T_e	Engine torque
T_w	Viscous torque on wheel
F_a	Longitudinal aerodynamic drag force
F_f	Longitudinal tire force
λ	Longitudinal slip
μ	Longitudinal friction coefficient
ζ	Aerodynamic drag constant
ρ	Viscous friction in driven wheel
P	Master cylinder pressure
r	Wheel radius
m	Vehicle mass
l	Wheel base length
l_r	distance from gravity center to rear wheel
g	Gravity acceleration
h	Gravity center height

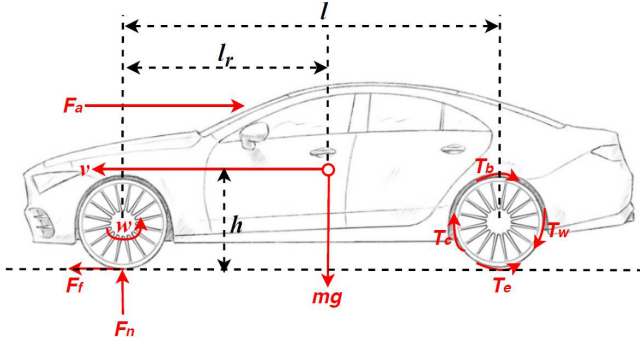


Figure 1. Front-wheel-driven vehicle model.

B. Vehicle Model

The longitudinal vehicle model is depicted in Figure 1, whose control variables are engine torque and master cylinder pressure, respectively. We make the following assumption on the vehicle's model throughout this paper.

Assumption 1: The vehicle's

- 1) dynamics of the left and the right sides are identical (i.e. the vehicle is symmetric);
- 2) wheel is damped with a viscous torque [34], i.e.,

$$T_w(t) = \rho w(t); \quad (1)$$

- 3) longitudinal aerodynamic drag force can be linearized in terms of longitudinal velocity [34], i.e.,

$$F_a(t) = \zeta v(t). \quad (2)$$

The uncertainties pertaining to the relations (1) and (2) are included in the following dynamics of the vehicle's longitudinal and wheel motions on a flat road, [26]:

$$J\dot{w}(t) = T_e(t) - T_w(t) - T_b(t) - T_c(t) + \tilde{f}_w(t), \quad (3a)$$

$$m\dot{v}(t) = \frac{T_c(t)}{r} - F_a(t) + \tilde{f}_v(t), \quad (3b)$$

where $\tilde{f}_w(t)$ and $\tilde{f}_v(t)$ represent uncertainties that are due to the modeling errors, noise, disturbances, unmodeled forces/torques in (1), (2), and others.

Following [11], the actual relation between the master cylinder pressure and the brake torque is modeled by a linear model with uncertainty:

$$T_b(t) = C\eta_b r_b P(t) + \varpi_b(t), \quad (4)$$

where C , η_b and r_b denote the known brake piston effective area, pad friction coefficient and brake disc effective radii, respectively; and the unknown $\varpi_b(t)$ denotes the uncertainty.

The wheel slip defined in term of wheel and longitudinal velocities as

$$s \triangleq \begin{cases} v - wr, & \text{if } v \geq wr \\ wr - v, & \text{if } v < wr \end{cases} \quad (5)$$

is the control objective of TCS [6]. We note that $s = 0$ and $s = \max\{v, wr\}$ indicate pure rolling and full sliding, respectively. In this paper, the slip will be imposed on velocity tracking control as a safety constraint.

We now define a set of driving environment indices:

$$\mathbb{E} \triangleq \{\text{dry, wet, snow, } \dots, \text{icy}\}, \quad \mathbb{U} \triangleq \mathbb{E} \cup \{\text{learned}\}. \quad (6)$$

Remark 1: \mathbb{E} is regarded as the set of normal environments, whose elements have the corresponding off-line-built vehicle models, while the element 'learned' in \mathbb{U} denotes the unforeseen driving environment, whose corresponding vehicle model needs to be learnt from limited velocity sensor data.

The experimental data of tire friction models shows that the tire friction torque depends on slip (or slip ratio) and road friction coefficient [6], [7]. We also use a linear model with uncertainty to describe the actual relation between the tire friction torque, slip and road friction coefficient, i.e., $T_c(t) = k_{\sigma(t)}s(t) + \varpi_c(t)$, where $k_{\sigma(t)}$ is obtained from experimental data via parameter identification, $\varpi_c(t)$ denotes the unknown uncertainty, and $\sigma(t) \in \mathbb{E}$, where, e.g., $\sigma(t) = \text{'snow'}$ for $t \in [t_k, t_{k+1})$ means the vehicle is driving in the snow environment during the time interval $[t_k, t_{k+1})$. With the consideration of (5), $T_c(t)$ is equivalently expressed as

$$T_c(t) = \begin{cases} (\frac{v(t)}{r} - w(t))k_{\sigma(t)} + \varpi_c(t), & \text{if } v(t) \geq w(t)r \\ (w(t) - \frac{v(t)}{r})k_{\sigma(t)} + \varpi_c(t), & \text{if } v(t) < w(t)r \end{cases}$$

substituting which together with (1), (2) and (4) into (3) yields a vehicle model with uncertainties:

- if $v(t) \geq w(t)r$,

$$\dot{w}(t) = \frac{k_{\sigma(t)} - \rho}{J} w(t) - \frac{k_{\sigma(t)}}{Jr} v(t) + u(t) + f_w(t), \quad (7a)$$

$$\dot{v}(t) = -\frac{k_{\sigma(t)}}{mr} w(t) + \frac{k_{\sigma(t)} - \zeta r^2}{mr^2} v(t) + f_v(t); \quad (7b)$$

- if $v(t) < w(t)r$,

$$\dot{w}(t) = -\frac{k_{\sigma(t)} + \rho}{J} w(t) + \frac{k_{\sigma(t)}}{Jr} v(t) + u(t) + f_w(t), \quad (8a)$$

$$\dot{v}(t) = \frac{k_{\sigma(t)}}{mr} w(t) - \frac{k_{\sigma(t)} + \zeta r^2}{mr^2} v(t) + f_v(t); \quad (8b)$$

where $u(t)$ denotes control input ($u(t) > 0$ and $u(t) < 0$ indicate activated drive and brake models, respectively), and

$$u(t) = \frac{T_e(t) - C\eta_b r_b P(t)}{J}, \quad f_v(t) = \frac{\varpi_c(t) + r\tilde{f}_v(t)}{mr},$$

$$f_w(t) = -\frac{\varpi_c(t) + \varpi_b(t) + \tilde{f}_w(t)}{J}.$$

C. Variant \mathcal{L}_1 -Simplex Architecture

This subsection introduces the proposed \mathcal{L}_1 Simplex architecture with incorporation of switching control and finite-time model learning, which is adopted from [25]. As described by Figures 2 and 3, the proposed \mathcal{L}_1 -Simplex architecture for autonomous vehicles includes

- High-Performance Controller (HPC) (Figure 2): The HPC is a complex controller for the autonomous vehicle, which provides high levels of performance and advanced functionalities, and is active during normal operation of the system, due to which, it may not be fully verified.

- \mathcal{L}_1 -Based Robust High-Assurance Controller (RHAC) (Figures 2 and 3): The HAC is a *simple and verified* controller that provides limited levels of performance and reduced functionalities to guarantee safe and stable operation of the vehicle. As highlighted in Figure 3, the latest version includes
 - stored off-line-built vehicle models that vary with environment, which guarantee safe autonomous velocity regulation in dynamic normal driving environments;
 - finite-time model learning, which timely learns and updates the vehicle model for safe autonomous velocity regulation in unforeseen driving environments;
 - switching logic that depends on driving environment detection and real-time verification of the safety envelope, which is responsible for activating an off-line-built model or finite-time model learning for \mathcal{L}_1 adaptive controller.
- Uncertainty Monitor (Figure 2): This *verified* monitor takes the form of the state predictor in \mathcal{L}_1 adaptive control architecture, which provides estimates of the uncertainties inside the vehicle system with fast adaptation.
- Decision Logic (Figure 2): This *verified* logic depends on the magnitudes of uncertainty estimations and safety envelope, which triggers the switching from HPC to RHAC in the event of software and/or physical failures. Its real-time verification of the safety envelope and uncertainty measurement are also the input of the switching logic in RHAC (Figure 3) that activates stored vehicle models or model learning.

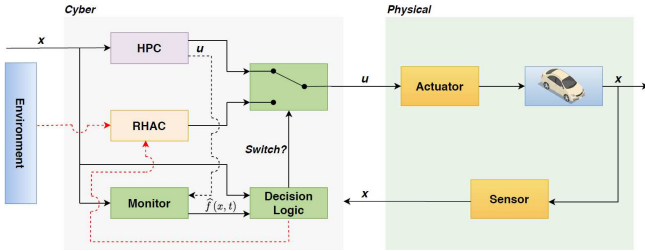


Figure 2. \mathcal{L}_1 -Simplex architecture.

Remark 2: In \mathcal{L}_1 -Simplex architecture, finite-time model learning is running in parallel with RHAC and HPC, which is depicted in Figure 3. This configuration guarantees when model learning is needed for reliable decision making, an inferred model is available immediately, so that RHAC is always in control. Without the configuration of parallel running, the car can lose control in unforeseen environment, which is due to the time delay in obtaining the inferred vehicle model from model learning and then the updating safe controllers.

As shown in Figures 2 and 3, the proposed \mathcal{L}_1 Simplex includes three types of switching: 1) switching between HPC and RHAC, 2) switching between stored vehicle models and inferred vehicle from model learning, and 3) switching between two subsystems in a fixed environment. To exclude Zeno behaviors in switching logic, we impose a minimum dwell

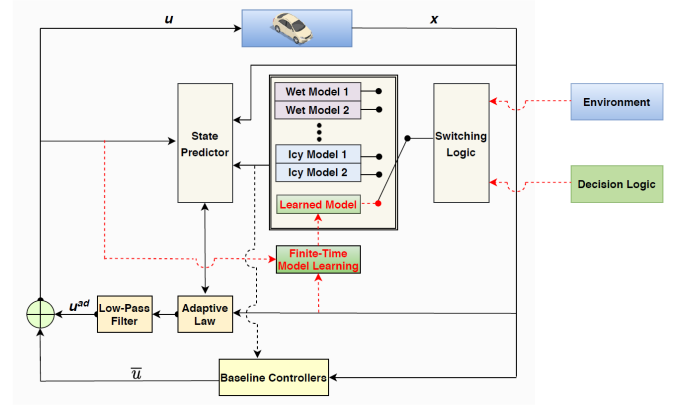


Figure 3. \mathcal{L}_1 -based RHAC architecture with switching control and finite-time model learning.

time on HPC, RHAC, learned vehicle models and stored sub-models, i.e.,

$$\min_{\forall k \in \mathbb{N}_0} \{t_{k+1} - t_k\} \geq \text{dwell}_{\min} > 0, \quad (9)$$

where t_k denotes the switching time.

Remark 3: The reliable environmental perception is the key to the fast and accurate detection of driving environments, which however is beyond the scope of this paper. Instead, we make a corresponding assumption on the capability of intelligent vehicle.

Assumption 2: The vehicle is equipped with sensors for real-time environmental perception, which can accurately detect the driving environments.

The proposed \mathcal{L}_1 -Simplex with switching control and finite-time model learning has two safe control objectives, which are formally stated below.

- **Safe Control Objective I:** the vehicle asymptotically steers its velocity to the provided varying references, while restricts its wheel slips to allowable safe sets in dynamic and unforeseen driving environments.
- **Safe Control Objective II:** the vehicle control system tolerates the concurrent software and physical failures.

This paper mainly focuses on \mathcal{L}_1 -based RHAC, since the two safe control objectives are primarily achieved by the RHAC. In the following, we will first present the formula of safety envelope pertaining to wheel slip. We then present the off-line-built vehicle models and inferred vehicle model via model learning, and the corresponding safe switching control, which will pave the way to RHAC design.

III. SAFETY ENVELOPES

This paper considers velocity regulation via tracking the provided references in two different scenarios that are

- Varying velocity references with respect to normal driving environments, i.e.,

$$\exists \sigma, \epsilon \in \mathbb{E}, \quad \mathbf{v}_\sigma^r \neq \mathbf{v}_\epsilon^r \text{ and } \mathbf{w}_\sigma^r \neq \mathbf{w}_\epsilon^r \quad (10)$$

- Zero velocity reference in unforeseen driving environments, i.e.,

$$\sigma = \text{learned}, \quad \mathbf{v}_\sigma^r = \mathbf{w}_\sigma^r = 0, \quad (11)$$

where \mathbf{v}_σ^r and \mathbf{w}_σ^r , respectively, denote the longitudinal and angular velocity references for driving environment $\sigma \in \mathbb{U}$, and \mathbb{U} and \mathbb{E} are given in (6).

Remark 4: In the unforeseen driving environments, see e.g., 2019 New York City Snow Squall [27], the possible sudden slick conditions on roadways, rapidly reduced visibility, unforecast adverse weather conditions, etc., can lead to high speed wrecks, pile ups, and subsequently injuries and fatalities. The safety strategy for autonomous vehicles driving in these environments should be safe parking on a road side, rather than continuous driving, which is the motivation behind the zero velocity reference in unforeseen environments.

For **Safe Control Objective I**, the provided velocity references are required to satisfy the following condition:

$$\mathbf{v}_\sigma^r - r\mathbf{w}_\sigma^r - \frac{\zeta r^2 \mathbf{v}_\sigma^r}{k_\sigma} = 0, \quad \mathbf{v}_\sigma^r \geq r\mathbf{w}_\sigma^r, \quad \sigma \in \mathbb{U} \quad (12a)$$

$$r\mathbf{w}_\sigma^r - \mathbf{v}_\sigma^r - \frac{\zeta r^2 \mathbf{v}_\sigma^r}{k_\sigma} = 0, \quad \mathbf{v}_\sigma^r < r\mathbf{w}_\sigma^r, \quad \sigma \in \mathbb{U}, \quad (12b)$$

based on which we define the tracking error vector:

$$e^\top(t) \triangleq [e_w(t), e_v(t)] = [w(t), v(t)] - [\mathbf{w}_{\sigma(t)}^r, \mathbf{v}_{\sigma(t)}^r]. \quad (13)$$

Remark 5: The relation (12) indicates that the desired slip is $s^r = \mathbf{v}_\sigma^r - r\mathbf{w}_\sigma^r = \frac{\zeta r^2 \mathbf{v}_\sigma^r}{k_\sigma}$, which depends on driving environment indexed by σ . Instead of regulating the wheel slip to the desired s^r , we are interested in restricting the slip to a safety set, which will be a constraint condition for safe control design.

In addition to velocity regulation for collision avoidance, lane keeping, and other constraints, the wheel slip s (defined in (5)) should be below a safety boundary (which varies with driving environment) to prevent slipping and sliding, i.e.,

$$s = |wr - v| \leq \mu_\sigma. \quad (14)$$

Substituting (12) into (14) yields

$$\begin{aligned} |wr - v| &= \left| wr - v - \mathbf{w}_\sigma^r r + \mathbf{v}_\sigma^r + \frac{\zeta r^2 \mathbf{v}_\sigma^r}{k_\sigma} \right| \\ &= \left| e_v - e_w r - \frac{\zeta r^2 \mathbf{v}_\sigma^r}{k_\sigma} \right| \leq \mu_\sigma, \quad \mathbf{v}_\sigma^r < r\mathbf{w}_\sigma^r, \quad \sigma \in \mathbb{U} \end{aligned} \quad (15)$$

$$\begin{aligned} |wr - v| &= \left| v - wr - \mathbf{v}_\sigma^r + r\mathbf{w}_\sigma^r + \frac{\zeta r^2 \mathbf{v}_\sigma^r}{k_\sigma} \right| \\ &= \left| e_v - e_w r + \frac{\zeta r^2 \mathbf{v}_\sigma^r}{k_\sigma} \right| \leq \mu_\sigma, \quad \mathbf{v}_\sigma^r \geq r\mathbf{w}_\sigma^r, \quad \sigma \in \mathbb{U} \end{aligned} \quad (16)$$

which are equivalently expressed as

- if $\mathbf{v}_\sigma^r \geq \mathbf{w}_\sigma^r r$,

$$-\mu_\sigma - \frac{\zeta r^2 \mathbf{v}_\sigma^r}{k_\sigma} \leq e_v - e_w r \leq \mu_\sigma - \frac{\zeta r^2 \mathbf{v}_\sigma^r}{k_\sigma}; \quad (17)$$

- if $\mathbf{v}_\sigma^r < \mathbf{w}_\sigma^r r$,

$$-\mu_\sigma + \frac{\zeta r^2 \mathbf{v}_\sigma^r}{k_\sigma} \leq e_v - e_w r \leq \mu_\sigma + \frac{\zeta r^2 \mathbf{v}_\sigma^r}{k_\sigma}. \quad (18)$$

Based on (17) and (18), we define a set of vectors:

$$\hat{c}_\sigma \triangleq \left[\frac{r k_\sigma}{\zeta r^2 \mathbf{v}_\sigma^r - \mu_\sigma k_\sigma}, \frac{k_\sigma}{\mu_\sigma k_\sigma - \zeta r^2 \mathbf{v}_\sigma^r} \right]^\top, \quad (19)$$

by which we obtain the following lemma regarding safety formula, whose proof is given in Appendix A.

Lemma 1: Consider the vector (19). The safety condition (14) holds if

$$-1 \leq \hat{c}_\sigma^\top e \leq 1, \quad (20)$$

where e and \hat{c} are defined in (13) and (19), respectively.

Building on (20), safety constraint set for ideal vehicle models is defined as follows:

$$\Omega_\sigma \triangleq \{e \in \mathbb{R}^2 \mid c_\sigma^\top e \leq 1\}, \quad \sigma \in \mathbb{U}, \quad (21)$$

where we define

$$c_\sigma^\top \triangleq \begin{cases} \hat{c}_\sigma, & \text{if } v \geq wr \\ -\hat{c}_\sigma, & \text{if } v < wr. \end{cases} \quad (22)$$

In addition, we define the following invariant sets and boundary sets, which will be used to determine the safety envelopes:

$$\Phi_\sigma \triangleq \{e \in \mathbb{R}^2 \mid e^\top \bar{P}_\sigma e \leq 1\}, \quad \sigma \in \mathbb{U} \quad (23)$$

$$\partial\Phi_\sigma \triangleq \{e \in \mathbb{R}^n \mid e^\top \bar{P}_\sigma e = 1\}, \quad \sigma \in \mathbb{U}, \quad (24)$$

where

$$\bar{P}_\sigma = \begin{bmatrix} \bar{p}_1^\sigma & & \\ & \bar{p}_2^\sigma & \\ & & \bar{p}_3^\sigma \end{bmatrix} > 0. \quad (25)$$

The following lemma provides a condition under which Φ_σ is a subset of safety set Ω_σ , which will be used for safe autonomous velocity regulation.

Lemma 2: Consider the safety sets (21) and (23). $\Phi_\sigma \subseteq \Omega_\sigma$ holds if and only if $\hat{c}_\sigma^\top \bar{P}_\sigma^{-1} \hat{c}_\sigma \leq 1$, $\sigma \in \mathbb{U}$.

Proof: It is straightforward to verify from (22) that $c_\sigma^\top \bar{P}_\sigma^{-1} c_\sigma = \hat{c}_\sigma^\top \bar{P}_\sigma^{-1} \hat{c}_\sigma$. Then, the rest of the proof is the same as that of Lemma 4.1 in [35]; here it is omitted. ■

Building on Lemma 2, the safety invariant set (23) and the safety boundary set (24), we present the safety envelopes for vehicles driving in different environments:

$$\Theta_\sigma \triangleq \{e \in \mathbb{R}^2 \mid e^\top \bar{P}_\sigma e \leq \theta \text{ and } \min_{y \in \partial\Phi_\sigma} \|e - y\| \geq \varepsilon\}, \quad (26)$$

where $\theta < 1$ and $\varepsilon < 1$.

IV. VEHICLE MODEL REFERENCES

As shown in Figure 3, \mathcal{L}_1 -based RHAC needs to store several off-line-built vehicle model references that correspond to different environments, as well as the learned model reference from finite-model leaning in an unforeseen driving environment, for state predictor and baseline controllers design. We note from (7) and (8) that real vehicle models under each fixed road $\sigma \in \mathbb{E}$ have two subsystems that are determined by internal state-dependent switching rules, i.e., $v(t) \geq w(t)r$ and $v(t) < w(t)r$. We now define a set of overall switching indices:

$$\mathbb{S} \triangleq \{\text{hpc}, \text{learned}, \text{dry}^1, \text{dry}^2, \text{wet}^1, \text{wet}^2, \dots, \text{icy}^1, \text{icy}^2\}, \quad (27)$$

where ‘learned’ denotes the learned model reference in an unforeseen environment, ‘hpc’ denoted the vehicle system under the control from HPC, ‘icy¹’ and ‘icy²’ denote the vehicle models under the conditions of $v(t) \geq w(t)r$ and $v(t) < w(t)r$ in the ice environment, respectively.

A. Off-Line-Built Vehicle Model References

The off-line-built model references are straightforwardly obtained from (7) and (8) via dropping uncertainties as follows:

- if $v(t) \geq w(t)r$,

$$\dot{\bar{w}}(t) = \frac{k_{\sigma(t)} - \varrho}{J} \bar{w}(t) - \frac{k_{\sigma(t)}}{Jr} \bar{v}(t) + \bar{u}(t), \quad (28a)$$

$$\dot{\bar{v}}(t) = -\frac{k_{\sigma(t)}}{mr} \bar{w}(t) + \frac{k_{\sigma(t)} - \zeta r^2}{mr^2} \bar{v}(t); \quad (28b)$$

- if $v(t) < w(t)r$,

$$\dot{\bar{w}}(t) = -\frac{k_{\sigma(t)} + \varrho}{J} \bar{w}(t) + \frac{k_{\sigma(t)}}{Jr} \bar{v}(t) + \bar{u}(t), \quad (29a)$$

$$\dot{\bar{v}}(t) = \frac{k_{\sigma(t)}}{mr} \bar{w}(t) - \frac{k_{\sigma(t)} + \zeta r^2}{mr^2} \bar{v}(t). \quad (29b)$$

We now define:

$$x \triangleq [w, v]^\top, \bar{x} \triangleq [\bar{w}, \bar{v}]^\top, f_0 \triangleq [f_w, f_v]^\top, B \triangleq [1, 0]^\top, \quad (30a)$$

$$A_{\sigma^1} \triangleq \begin{bmatrix} \frac{k_{\sigma(t)} - \varrho}{J} & -\frac{k_{\sigma(t)}}{Jr} \\ -\frac{k_{\sigma(t)}}{mr} & \frac{k_{\sigma(t)} - \zeta r^2}{mr^2} \end{bmatrix}, A_{\sigma^2} \triangleq \begin{bmatrix} -\frac{k_{\sigma(t)} + \varrho}{J} & \frac{k_{\sigma(t)}}{Jr} \\ \frac{k_{\sigma(t)}}{mr} & -\frac{k_{\sigma(t)} + \zeta r^2}{mr^2} \end{bmatrix}. \quad (30b)$$

With these definitions at hand, the real vehicle dynamics described by (7) and (8), and the vehicle model reference described by (28) and (29) are, respectively, rewritten as

$$\dot{x}(t) = A_{\bar{\sigma}(t)} x(t) + Bu(t) + f_0(x, t), \quad \tilde{\sigma}(t) \in \mathbb{S} \quad (31)$$

$$\dot{\bar{x}}(t) = A_{\tilde{\sigma}(t)} \bar{x}(t) + B\bar{u}(t), \quad \tilde{\sigma}(t) \in \mathbb{S}_{/\{\text{hpc, learned}\}}, \quad (32)$$

where \mathbb{S} is given in (27), $\bar{x}(t_0) = x(t_0)$ with t_0 denoting the initial time. The definition (27), in conjunction with (6), shows that the relation between $\tilde{\sigma}(t)$ and $\sigma(t)$ can be described by

$$\text{For } \tilde{\sigma}(t) \in \mathbb{S}_{/\{\text{hpc, learned}\}}, \tilde{\sigma}(t) = \sigma^i(t), i \in \{1, 2\}, \sigma(t) \in \mathbb{E}. \quad (33)$$

Remark 6: We handle the unmodeled forces/torques, e.g., rolling resistance forces, as uncertainties, which will be compensated by \mathcal{L}_1 adaptive controller in RHAC.

B. Finite-Time Model Learning

1) *Model Learning Procedure:* The unknown and unmeasured environmental characteristics can potentially lead to large mismatch between the off-line-built vehicle-environment interaction model references and real vehicle behaviors in unforeseen environments. Subsequently, the control action cannot be reliable. This motivates to employ finite-time model learning to infer a vehicle model reference using limited sensor data generated in the unforeseen environment. When model learning is triggered, RHAC transforms to a model-learning based control, whose framework is briefly described in Figure 4. Since control input matrix B given in (30a) does not include any vehicle parameters, learning a system matrix is sufficient for \mathcal{L}_1 -based RHAC.

The data sampling technique transforms the continuous-time dynamics to be discrete-time. The discretization of real system (31) is thus obtained as

$$x(p+1) = (\mathbf{I} + TA_{\bar{\sigma}(p)}) x(p) + TBu(p) + Tf_0(x, p), \quad (34)$$

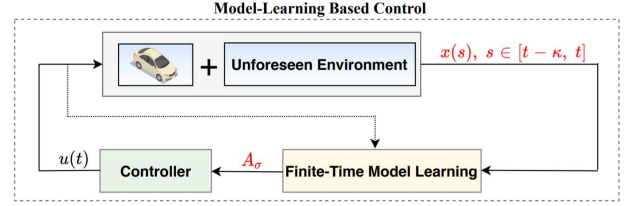


Figure 4. Finite-time model-learning based control architecture.

where $p \in \{k, k+1, \dots, k+m\}$, with T being the sampling period, and

$$k = \frac{t - \kappa}{T}, \quad m = \frac{\kappa}{T}, \quad (35)$$

such that $kT = t - \kappa$ and $(k+m)T = t$.

Following the learning procedure developed [33], the finite-time model learning algorithm is introduced as:

$$(\mathbf{I} + TA_{\text{learned}}) \bar{P} = \bar{Q} + \bar{R}, \quad (36)$$

where we define

$$\bar{P} \triangleq \sum_{p=k}^{k+m-2} (x(p) - x(p+1))(x(p) - x(p+1))^\top, \quad (37)$$

$$\bar{Q} \triangleq \sum_{p=k}^{k+m-2} (x(p+1) - x(p+2))(x(p) - x(p+1))^\top, \quad (38)$$

$$\bar{R} \triangleq \sum_{p=k}^{k+m-2} TB(u(p) - u(p-1))(x(p) - x(p+1))^\top. \quad (39)$$

From the discrete-time computation (36), we in turn obtain the continuous-time vehicle model reference:

$$\dot{\bar{x}}(t) = A_{\text{learned}} \bar{x}(t) + B\bar{u}(t), \quad (40a)$$

$$A_{\text{learned}} = \frac{1}{T} ((\bar{Q} + \bar{R}) \bar{P}^{-1} - \mathbf{I}). \quad (40b)$$

Remark 7 (Unforeseen Environmental Data): The switching logic pertaining to learned model reference, which is formally presented in Section VI, depends on environmental perception and real-time verification of the safety envelope and uncertainty measurement. Specifically, if the perception detects the occurrence of unforeseen environment, but the vehicle's real-time state does not deviate from the safety envelope and the magnitude of uncertainty measurement does not exceed a preset threshold, the learned model reference will not be activated. This switching logic implies that the recorded data $x(s)$, $s \in [t - \kappa, t]$, for the learned model reference activated at current time t , already includes the sensor data generated in the unforeseen environment.

Remark 8 (Parallel Running): As shown in Figure 4 or the relation (35), the HPC, RHAC and finite-time model learning are running in parallel, such that once the model learning solution is needed, an inferred matrix A_{learned} is available immediately for safety controller updating.

2) *Sample Complexity Bounds, Sampling Period and Observation Horizon*: The sample complexity bounds on model learning procedure (36) when $TBu(p) + Tf_0(x, p)$ in (34) can be modeled by a random vector are derived in [33]. It includes the upper bounds on the number of observations sufficient to identify system matrix with prescribed levels of accuracy and confidence. As indicated by (35), this upper bound can be achieved through adjustment of the sampling period T . To review the influence of sampling period T on the sample complexity bounds, let us consider a simplified discrete system that can represent (34) at some extent:

$$\mathbf{x}(p+1) = A\mathbf{x}(p) + \mathbf{f}(p), \quad (41a)$$

$$\mathbf{r}(p) = \mathbf{x}(p) + \mathbf{w}(p), \quad p \in \mathbb{N} \quad (41b)$$

where $\mathbf{f}(p)$ and $\mathbf{w}(p)$, respectively, denote the process and observation noise.

The learned matrix that follows learning procedure (36) for the system (41) updates as

$$A_i = \widehat{Q}\widehat{P}^{-1} \quad (42a)$$

$$\widehat{P} = \sum_{p=k}^{k+m-2} (\mathbf{r}(p) - \mathbf{r}(p-1))(\mathbf{r}(p) - \mathbf{r}(p-1))^\top \quad (42b)$$

$$\widehat{Q} = \sum_{p=k}^{k+m-2} (\mathbf{r}(p+1) - \mathbf{r}(p))(\mathbf{r}(p) - \mathbf{r}(p-1))^\top \quad (42c)$$

We can obtain the dynamics of noisy observation from the real system (41):

$$\mathbf{r}(p) = A\mathbf{r}(p-1) + \mathbf{h}(p), \quad \mathbf{r}(1) = \mathbf{x}(1) + \mathbf{w}(1), \quad p \geq 2 \in \mathbb{N}. \quad (43)$$

where

$$\mathbf{h}(p) \triangleq \mathbf{f}(p) + \mathbf{w}(p) - A\mathbf{w}(p-1), \quad p \geq 2 \in \mathbb{N}. \quad (44)$$

Remark 9: We have proved in [33] that compared with ordinary least-square estimator, the proposed learning procedure (42) has smaller estimation error of system matrix when the observation noise has non-zero mean, and compared with naive least-square estimator, the inference feasibility of (42) is more robust to observation-starting time and data length. However, the recently derived sample complexity bounds for ordinary least-square estimator in [28]–[32] do not hold for the procedure (42), which can be explained by the following observations:

- even assuming both $\mathbf{f}(p)$ and $\mathbf{w}(p)$ are drawn independently and have independent coordinates, due to $A\mathbf{w}(k-1)$, the processed random vector $\mathbf{h}(p)$ has dependencies on coordinates and time;
- the obtained sample complexity bounds in [28]–[31] rely on the assumption that $\mathbf{h}(p)$ has independence on coordinates and time.

Through leveraging the variant Hanson-Wright inequality for random vectors with dependencies, we derived the sample complexity bounds on (42), which is formally presented in the following theorem. We refer reader to [33] for its assumption and parameter notations.

Theorem 1: [33] Consider the system (43) and learned matrix in (42). For any $0 < \bar{\delta} < 1$, and any $\bar{\phi} > 0$, we

have: $\mathbf{P}(\|A - A_i\| \leq \bar{\phi}) \geq 1 - \bar{\delta}$, as long as the following conditions hold

$$\min \left\{ \frac{\bar{\rho}^2}{4\|C_v^{-0.5}\|_F^2\|C_v\|}, \frac{\bar{\rho}}{2\|C_v^{-0.5}\|_F^2} \right\} \geq \frac{\bar{\gamma}^2}{2} \ln \frac{4 \cdot 9^n}{\bar{\delta}}, \quad (45)$$

$$\lambda_{\min}(\Upsilon_{(k,m)}) \geq \frac{16\bar{\gamma}^2}{(1-\bar{\rho})\bar{\phi}^2} \ln \left(\frac{\sqrt{2} \cdot 5^n}{\bar{\delta}} \left(\frac{1-\bar{\rho}}{10} \right)^{0.5n} \right), \quad (46)$$

where $0 < \rho < 1$, and

$$\Upsilon_{(k,m)} = (2\sigma_\delta^2 + \sigma_{\bar{p}}^2)m\mathbf{I} + \sum_{p=k}^{k+m-1} \sum_{i=0}^{p-3} A^i(\mathbf{I}-A)(\mathbf{I}-A)^\top (A^i)^\top \sigma_{\bar{p}}^2.$$

Remark 10: As indicated by the conditions (45) and (46), a rough upper bound on number of observations can be obtained as

$$m_{\text{up}} = \frac{16\bar{\gamma}^2}{(1-\bar{\rho})\bar{\phi}^2(2\sigma_\delta^2 + \sigma_{\bar{p}}^2)} \ln \left(\frac{\sqrt{2} \cdot 5^n}{\bar{\delta}} \left(\frac{1-\bar{\rho}}{10} \right)^{0.5n} \right),$$

such that (46) holds for any $m \geq m_{\text{up}}$. Under the constraint (45), the lower bound on model error $\bar{\phi}$ can also be implicitly estimated from (46) through

$$\bar{\phi}_{\text{lo}}^2 = \frac{16\bar{\gamma}^2}{(1-\bar{\rho})\lambda_{\min}(\Upsilon_{(m,l)})} \ln \left(\frac{\sqrt{2} \cdot 5^n}{\bar{\delta}} \left(\frac{1-\bar{\rho}}{10} \right)^{0.5n} \right).$$

If $Tf_0(x, p)$ in (34) can be modeled by the random vector under the imposed assumption in [33], the complexity bounds can be applied to the model learning procedure (36) to for optimal sampling time period T and observation horizon κ for the prescribed levels of accuracy and confidence, since the number of observations m is determined by the sampling period and the horizon, which is implied by (35).

Remark 11: If $Tf_0(x, p)$ in (34) cannot be modeled by the random vector in [33], the obtained complexity bounds may not be applicable to (40). The learned system matrix can still be used by \mathcal{L}_1 -Simplex, since \mathcal{L}_1 adaptive controller compensates for the identification error included in uncertainties.

V. SAFE SWITCHING CONTROL

This section investigates safe switching control of off-line-built and learned vehicle model references. We now define the tracking error vector for model references:

$$\bar{\mathbf{e}}^\top \triangleq [\bar{\mathbf{e}}_w, \bar{\mathbf{e}}_v] = [\bar{\mathbf{w}}, \bar{\mathbf{v}}] - [\mathbf{w}_\sigma^r, \mathbf{v}_\sigma^r]. \quad (47)$$

The velocity tracking control for the off-line-built model reference (32) and finite-time learned model reference (40) is given as follows:

$$\bar{\mathbf{u}} = \begin{cases} -F_\sigma^w \bar{\mathbf{e}}_w - F_\sigma^v \bar{\mathbf{e}}_v + \frac{\zeta r \mathbf{v}_\sigma^r + \rho \mathbf{w}_\sigma^r}{J}, & \bar{\sigma} \in \mathbb{S} \setminus \{\text{hpc, learned}\} \\ -F_\sigma^w \bar{\mathbf{w}} - F_\sigma^v \bar{\mathbf{v}} = -F_\sigma^w \bar{\mathbf{e}}_w - F_\sigma^v \bar{\mathbf{e}}_v, & \bar{\sigma} \in \{\text{learned}\} \end{cases}, \quad (48)$$

where \mathbb{S} is given in (27), F_σ^w and F_σ^v are the designed control gains.

In the following, we start from a simple case of identical velocity reference that includes (11), i.e.,

$$\forall \sigma \in \mathbb{U}, \quad \mathbf{v}_\sigma^r = \mathbf{v}^r \text{ and } \mathbf{w}_\sigma^r = \mathbf{w}^r. \quad (49)$$

We then extend the results to the more general case (10).

A. Identical Velocity Reference

1) *Stabilization*: Substituting (12) under the constraint (49) into the models (32) and (40) with the control input (48) leads to the dynamics of tracking error (47):

$$\dot{\bar{e}}(t) = \widehat{A}_{\bar{\sigma}(t)}\bar{e}(t), \quad \bar{\sigma}(t) \in \mathbb{S}/\{\text{hpc}\}, \quad (50)$$

where \mathbb{S} is given in (27), and

$$\widehat{A}_{\sigma^1} = \begin{bmatrix} \frac{k_\sigma - \varrho}{J} - F_{\sigma^1}^w & -\frac{k_\sigma - F_{\sigma^1}^v}{J} \\ -\frac{k_\sigma}{mr} & \frac{k_\sigma - \zeta r^2}{mr^2} \end{bmatrix}, \quad \sigma \in \mathbb{E} \quad (51)$$

$$\widehat{A}_{\sigma^2} = \begin{bmatrix} -\frac{k_\sigma - \varrho}{J} - F_{\sigma^2}^w & \frac{k_\sigma - F_{\sigma^2}^v}{J} \\ \frac{k_\sigma}{mr} & -\frac{k_\sigma - \zeta r^2}{mr^2} \end{bmatrix}, \quad \sigma \in \mathbb{E} \quad (52)$$

$$\widehat{A}_{\text{learned}} = A_{\text{learned}} - B[F_{\text{learned}}^w, F_{\text{learned}}^v], \quad (53)$$

with \mathbb{E} defined in (6). The following theorem, whose proof appears in Appendix B, presents the stability of off-line-built system matrices.

Theorem 2: Consider the system matrices (51) and (52).

- The matrix \widehat{A}_{σ^1} is Hurwitz if and only if

$$F_{\sigma^1}^w > \frac{k_\sigma - \varrho}{J} - \frac{k_\sigma}{mr^2} - \frac{\zeta}{m}, \quad (54a)$$

$$F_{\sigma^1}^v < -\frac{\varrho}{rJ} + \frac{\zeta r^2 - k_\sigma}{rk_\sigma} F_{\sigma^1}^w - \frac{(k_\sigma - \varrho)\zeta r}{k_\sigma J}. \quad (54b)$$

- The matrix \widehat{A}_{σ^2} is Hurwitz if and only if

$$F_{\sigma^2}^w > -\frac{k_\sigma}{J} - \frac{\varrho}{J} - \frac{k_\sigma}{mr^2} - \frac{\zeta}{m}, \quad (55a)$$

$$F_{\sigma^2}^v > -\frac{\varrho}{rJ} - \frac{\zeta r^2 + k_\sigma}{rk_\sigma} F_{\sigma^2}^w - \frac{(k_\sigma + \varrho)\zeta r}{k_\sigma J}. \quad (55b)$$

Remark 12: When the aerodynamic drag force is ignored as studied in [6], the conditions (54) and (55) imply that if $F_{\sigma^1}^w = F_{\sigma^2}^w$, we have $F_{\sigma^1}^v \neq F_{\sigma^2}^v$, which means the identical control scheme (i.e., $F_{\sigma^1}^w = F_{\sigma^2}^w$ and $F_{\sigma^1}^v = F_{\sigma^2}^v$) cannot simultaneously stabilize the two subsystems driven by the switching conditions $v \geq wr$ and $v < wr$ (i.e., $\dot{\bar{e}}(t) = \widehat{A}_{\sigma^1}\bar{e}(t)$ and $\dot{\bar{e}}(t) = \widehat{A}_{\sigma^2}\bar{e}(t)$).

We note that there exists a class of switched systems, such that even when all of its subsystems are stable, the system can still be unstable if its switching time is not reasonable [36]. In the following lemma, whose proof is presented in Appendix C, we investigate whether this scenario can happen when the vehicle drives in a fixed environment. The answer will contribute to safe switching control design.

Lemma 3: For a fixed $\sigma \in \mathbb{E}$, if the control gains in the system matrices (51) and (52) satisfy (54) and (55), respectively, there exists a common $\bar{P}_\sigma > 0$ such that

$$\widehat{A}_{\sigma^i}^\top \bar{P}_\sigma + \bar{P}_\sigma \widehat{A}_{\sigma^i} < 0, \quad \forall i = 1, 2. \quad (56)$$

Remark 13: It directly follows from Theorem 3.4 of [36] that the switching time does not undermine the stability of ideal model (50) for a fixed $\sigma \in \mathbb{E}$, i.e., when driving in a fixed normal environment, under arbitrary switching (excluding Zeno behaviors) that is triggered by “ $v \geq wr$ ” and “ $v < wr$ ”, the switched system (50) is always stable.

2) *Safe Control*: With the consideration of (30b), and (51)–(53), the dynamics (50) can be equivalently transformed to

$$\dot{\bar{e}}(t) = (A_{\bar{\sigma}(t)} + \widehat{B}F_{\bar{\sigma}(t)})\bar{e}(t), \quad \bar{\sigma}(t) \in \mathbb{S}/\{\text{hpc}\}, \quad (57)$$

where $A_{\bar{\sigma}(t)}$ is given in (30b) and (40b), the control gains are included in matrix $F_{\bar{\sigma}(t)}$, which are to be computed, and

$$\widehat{B} \triangleq \begin{bmatrix} 1 & 1 \\ 0 & 0 \end{bmatrix}. \quad (58)$$

We next present the following LMI formula for obtaining $F_{\bar{\sigma}}$ and P_σ that guarantee safe autonomous velocity regulation:

$$Q_\sigma > 0, \quad \forall \sigma \in \mathbb{U} \quad (59a)$$

$$\check{c}_\sigma^\top Q_\sigma \check{c}_\sigma \leq 1, \quad \forall \sigma \in \mathbb{U} \quad (59b)$$

$$A_{\sigma^i} Q_\sigma + \widehat{B} \check{E}_{\sigma^i} + (A_{\sigma^i} Q_\sigma + \widehat{B} \check{E}_{\sigma^i})^\top < 0, \quad \forall \sigma \in \mathbb{E}, i = 1, 2 \quad (59c)$$

$$A_{\text{learned}} Q_{\text{learned}} + \widehat{B} \check{E}_{\text{learned}} + (A_{\text{learned}} Q_{\text{learned}} + \widehat{B} \check{E}_{\text{learned}})^\top < 0, \quad (59d)$$

based on which, we obtain

$$F_{\sigma^i} = \check{E}_{\sigma^i} \bar{P}_\sigma, \quad F_{\text{learned}} = \check{E}_{\text{learned}} \bar{P}_{\text{learned}}, \quad (60a)$$

$$\bar{P}_\sigma^{-1} = Q_\sigma, \quad \bar{P}_{\text{learned}}^{-1} = Q_{\text{learned}}, \quad i = 1, 2, \sigma \in \mathbb{E}, \quad (60b)$$

where \mathbb{E} and \mathbb{U} are defined in (6).

One potential benefit of switching control is extending the safety envelope to $\Theta = \bigcup_{\sigma \in \mathbb{U}} \Theta_\sigma$ [25]. However, the switching time is a critical factor in this extension. In other words, if the dwell times of subsystems are not reasonable, the safety envelope cannot be extended, which is illustrated by Figure 5:

- Figure 5 (a): at switching time t_{k+1} , the system state $\bar{e}(t_{k+1})$ does not fall into Θ_2 . Consequently, $\bar{e}(t) \notin \Theta$ for some time, which hinders the safety envelope extension.
- Figure 5 (b): at switching time t_{k+1} , the system state $\bar{e}(t_{k+1})$ falls into the safety envelope Θ_2 , which leads to $\Theta_2 \subseteq \Theta$, thus extends the safety envelope.

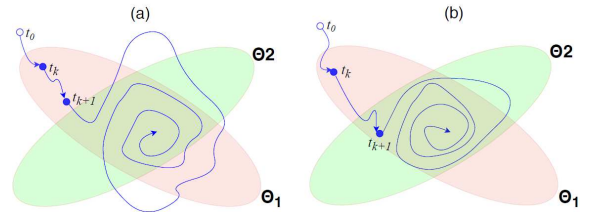


Figure 5. Phase plots under different scheduling of switching times.

We now define:

$$\bar{A}_{\sigma^i} \triangleq A_{\sigma^i} + BF_{\sigma^i}, \quad \bar{A}_{\text{learned}} \triangleq A_{\text{learned}} + BF_{\text{learned}}, \quad (61)$$

$$\lambda_{\max}^\sigma \triangleq \max_{i \in \{1, 2\}} \{\lambda_{\max}(\bar{P}_\sigma \bar{A}_{\sigma^i} + \bar{A}_{\sigma^i}^\top \bar{P}_\sigma)\}, \quad (62)$$

$$\lambda_{\max}^{\text{learned}} \triangleq \lambda_{\max}(\bar{P}_{\text{learned}} \bar{A}_{\text{learned}} + \bar{A}_{\text{learned}}^\top \bar{P}_{\text{learned}}). \quad (63)$$

With the definitions at hand, the following theorem presents the conditions on switching time that guarantee the system stability and the safety envelope extension simultaneously, whose proof is given in Appendix D.

Theorem 3: Consider the switched system (57) and safety envelopes (26), with $F_{\bar{\sigma}}$ and \bar{P}_{σ}^{-1} computed via (59) and (60). If the minimum dwell time satisfies

$$\text{dwell}_{\min} > \max_{p \neq q \in \mathbb{U}} \left\{ \frac{\lambda_{\max}(\bar{P}_p)}{\lambda_{\max}^p} \ln \frac{\lambda_{\min}(\bar{P}_q)}{\lambda_{\max}(\bar{P}_p)} \right\}, \quad (64)$$

the switched system (57) is stable, and $\bar{e}(t) \in \Theta = \bigcup_{\sigma \in \mathbb{U}} \Theta_{\sigma}$ for any $t \geq t_0$ if $\bar{e}(t_0) \in \Theta_{\sigma(t_0)}$.

B. Varying Velocity References

Substituting (12) under the constraints (10) and (11) into the model (32) with the control input (48) leads to the tracking error dynamics:

$$\dot{\bar{e}}(t) = (A_{\bar{\sigma}(t)} + \hat{B}F_{\bar{\sigma}(t)})\bar{e}(t), \quad t \in [t_k, t_{k+1}) \quad (65a)$$

$$\bar{e}(t_k) = E_k \bar{e}(t_k^-), \quad \bar{e}(t_0^+) = \bar{e}(t_0), \quad (65b)$$

where E_k is known matrix, $A_{\bar{\sigma}(t)}$ and \hat{B} are given by (30b) and (58), respectively.

The formula (65b) describes the impulsive effect induced by the ‘‘jumping’’ velocity reference at switching time. As illustrated by Figure 6, the impulsive effect has significant influence on the safety envelope extension, which would impose high requirement on minimum dwell time, and subsequently, safe control. The following theorem, whose proof appears in Appendix E, formally presents the safe control in this scenario.

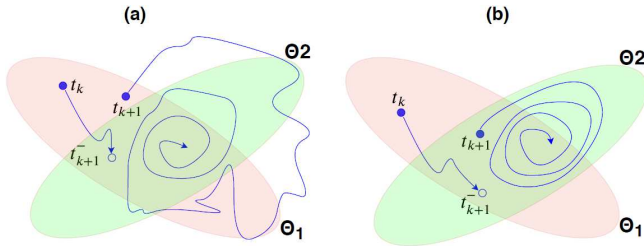


Figure 6. Impulsive effect on safety envelope: (a) system states escape from escape from safety envelope, (b) system states stay in safety envelope.

Theorem 4: Consider the switched system (65) and safety envelopes (26), with $F_{\bar{\sigma}}$ and \bar{P}_{σ}^{-1} computed via (59) and (60). If the minimum dwell time satisfies

$$\text{dwell}_{\min} > \max_{k \in \mathbb{N}} \left\{ \frac{\lambda_{\max}(\bar{P}_{\sigma(t_{k-1})})}{\lambda_{\max}^{\sigma(t_{k-1})}} \ln \frac{\lambda_{\min}(\bar{P}_{\sigma(t_{k-1})})}{\lambda_{\max}(E_k^{\top} \bar{P}_{\sigma(t_k)} E_k)} \right\}, \quad (66)$$

the switched system (65) is stable, and $\bar{e}(t) \in \Theta$ for any $t \geq t_0$ if $\bar{e}(t_0) \in \Theta_{\sigma(t_0)}$.

Remark 14 (Extension to Different Road Zones): The proposed safe switching control can be directly extended to the scenario of a fixed driving environment but different road zones, see e.g., school zone, commercial street, work zone in highway, etc. The switching set defined in (27) in this scenario updates as

$$\mathbb{S} \triangleq \{\text{hpc}, \text{school zone}^1, \text{school zone}^2, \dots\}.$$

VI. \mathcal{L}_1 -SIMPLEX DESIGN

Sections III–V, respectively, present the safety formula, off-line-built and learned vehicle model references and their safe switching control, which have paved the way to the design of new \mathcal{L}_1 -Simplex.

The dynamics of faulty vehicle system that corresponds to the real one in (31) operating in HPC is described by

$$\dot{x}(t) = A_{\text{hpc}}x(t) + Bu(t) + f_1(x, t), \quad (67)$$

where $f_1(x, t)$ is an uncertainty function that represents modeling errors, noise, disturbance, unmodeled forces/torques, etc. The fault dynamics (67) indicates that this paper focuses on the class of software and physical failures and unmodeled driving environments, whose influences can be modeled by $f_1(x, t)$.

This section studies the critical components in \mathcal{L}_1 -Simplex architecture, which relies on the following assumption on the uncertainty.

Assumption 3: The uncertainties $f_q(x, t)$ in (31) and (67) are uniformly bounded in time and Lipschitz in x over safety set, i.e., there exist positive l and b such that

$$\|f_q(0, t)\| \leq b_q, \quad (68a)$$

$$\|f_q(x_1, t) - f_q(x_2, t)\| \leq l_q \|x_1 - x_2\|, \quad q = 0, 1 \quad (68b)$$

hold for any $t \geq 0$, and $x_1 - [\mathbf{w}_{\sigma}^r, \mathbf{v}_{\sigma}^r]^{\top}$, $x_2 - [\mathbf{w}_{\sigma}^r, \mathbf{v}_{\sigma}^r]^{\top} \in \bigcup_{\sigma \in \mathbb{U}} \Omega_{\sigma}$, with Ω_{σ} given in (21).

In the following subsections, we present the critical components of \mathcal{L}_1 -Simplex in achieving **Safe Control Objective I** and **Safe Control Objective II** simultaneously.

A. Uncertainty Monitor

As shown in Figure 2, the decision logic needs the measurement of uncertainty from the monitor to make the decision of switching between HPC and RHAC. The dynamics of the uncertainty monitor of the real car under the control actuator from HPC is described by

$$\dot{z}(t) = A_z z(t) + (A_z B_z - B_z A_{\text{hpc}})x(t) - B_z B u(t), \quad (69a)$$

$$\hat{f}(x, t) = C_z z(t) + C_z B_z x(t), \quad (69b)$$

$$z(t_k) = -B_z x(t_k), \quad (69c)$$

where $\hat{f}(x, t) \in \mathbb{R}^2$ is a measurement of the uncertainty, and the triple (A_z, B_z, C_z) constitutes a low-pass filter [25].

B. Switching Rules

Building on the safety envelope (26), the uncertainty monitor (69), and the driving environment detection under Assumption 2, the switching rules that describe the decision logic for HPC and RHAC, and the switching logic for off-line-built and learned model references are described as below, where the decision logic is a minor revision of the one in [25].

- Decision Logic: switching from HPC to RHAC

– **Rule I:** triggered by the magnitude of uncertainty measurement:

$$\begin{aligned} & \|\hat{f}(x, t)\| \\ & > \int_0^t \|C_z e^{A_z(t-\tau)} B_z\| (l_0 \|x(\tau)\| + b_0) d\tau. \quad (70) \end{aligned}$$

- **Rule II:** triggered by the safety envelope (26):

$$e^\top(t)P_\sigma e(t) = \theta \text{ and } e^\top(t)P_\sigma \dot{e}(t) > 0, \forall \sigma \in \mathbb{U}. \quad (71)$$

- **Switching Logic:** switching from off-line-built models to learned model:

- **Rule III:** triggered by the uncertainty measurement (70) and environment detection $\sigma(t) \notin \mathbb{S}$.
- **Rule IV:** triggered by the safety envelope verification (71) and environment detection $\sigma(t) \notin \mathbb{S}$.

Remark 15: It has been proved in [25] that under (68) the triggering condition in **Rule I** does not hold, which indicates that RHAC is activated when the magnitude of uncertainty measurement exceeds a threshold.

C. \mathcal{L}_1 -Based RHAC

The components of \mathcal{L}_1 -based RHAC shown in Figure 3 are described in detail as follows.

1) *State Predictor:* The state predictor of RHAC in Figure 3 is described by

$$\dot{\tilde{x}}(t) = A_{\tilde{\sigma}(t)}x(t) + Bu(t) + \tilde{f}(t) - \alpha(\tilde{x}(t) - x(t)), \quad (72a)$$

$$\tilde{x}(t_{k^*}) = x(t_{k^*}), \quad (72b)$$

where t_{k^*} is the switching moment from HPC to RHAC, α is an arbitrary positive scalar, and $\tilde{f}(t)$ is the estimation of the uncertainties $f_0(x, t)$ and $f_1(x, t)$, which is computed by the following adaptation law.

2) *Adaptation Law:* The estimated $\tilde{f}(t)$ in (72) is computed via

$$\dot{\tilde{f}}(t) = K \text{Proj}_\Psi(\tilde{f}(t), -(\tilde{x}(t) - x(t))), \quad (73)$$

where K is the adaptive gain, and

$$\Psi = \left\{ f \in \mathbb{R}^2 \left| \|f\| \leq \rho = \frac{l}{\sqrt{\min_{\sigma \in \mathbb{U}} \{\lambda_{\min}(P_\sigma)\}}} + b \right. \right\}, \quad (74)$$

with

$$l = \max \{l_0, l_1\}, \quad b = \max \{b_0, b_1\}. \quad (75)$$

The projection operator $\text{Proj}_\Psi : \mathbb{R}^2 \times \mathbb{R}^2 \rightarrow \mathbb{R}^2$ in (73) is defined as

$$\text{Proj}_\Psi(p, q) \triangleq \begin{cases} q - \frac{\nabla g(p)(\nabla g(p))^\top q g(p)}{\|\nabla g(p)\|^2}, & \text{if } g(p) > 0 \text{ and } q^\top \nabla g(p) > 0 \\ q, & \text{otherwise} \end{cases} \quad (76)$$

where $g(p) = \frac{p^\top p - \rho^2 + 1 - \vartheta}{1 - \vartheta}$ with $\vartheta \in (1 - \rho^2, 1)$. It has been proved in [25] that the operator (76) can always guarantee $\tilde{f}(t) \in \Psi$.

3) *Low-Pass Filter:* The low-pass filter that takes $\tilde{f}(t)$ as control input is described by

$$\dot{\check{x}}(t) = \check{A}\check{x}(t) + \check{B}\tilde{f}(t), \quad (77a)$$

$$u^{\text{ad}}(t) = \check{C}\check{x}(t), \quad \check{x}(t_{k^*}) = \mathbf{0} \quad (77b)$$

where t_{k^*} denotes the switching time when RHAC is activated, the triple $(\check{A}, \check{B}, \check{C})$ is the state space realization of an 1×2 matrix of low-pass filters that are stable and strictly proper with the transfer function:

$$T(s) = \check{C}(s\mathbf{I} - \check{A})^{-1}\check{B}. \quad (78)$$

4) *Control Input of Real Vehicle:* As shown in Figure 3, the control input from RHAC for the real car in dynamic and unforeseen environments (31) is

$$u(t) = \hat{u}(t) - u^{\text{ad}}(t), \quad (79)$$

where $u^{\text{ad}}(t)$ is computed by (77), and

$$\hat{u}(t) = F_{\tilde{\sigma}(t)}\bar{e}(t) + \frac{1}{J} \begin{bmatrix} \varrho \mathbf{w}_{\sigma(t)}^\top \\ \zeta r \mathbf{v}_{\sigma(t)}^\top \end{bmatrix} \quad (80)$$

with $F_{\tilde{\sigma}(t)}$ given in (60).

D. Performance of \mathcal{L}_1 -Based RHAC

We first define:

$$H_{\tilde{\sigma}(t_k)}(s) \triangleq (s\mathbf{I} - A_{\tilde{\sigma}(t_k)} - \widehat{B}F_{\tilde{\sigma}(t_k)})^{-1},$$

$$\delta \triangleq \frac{\bar{e}^\top(t_{k^*})P_{\sigma(t_{k^*})}\bar{e}(t_{k^*})}{\lambda_{\min}(P_{\sigma(t_{k^*})})}, \quad (81)$$

$$\varepsilon \triangleq \frac{1}{(1 - \chi_{\tilde{\sigma}(t_k)})} \left(\|H_{\tilde{\sigma}(t_k)}(s)BT(s)(s + \alpha)\|_{\mathcal{L}_1} \sqrt{\frac{\mu}{K}} \right. \\ \left. + (\delta + \|x_{\tilde{\sigma}(t_k)}^*\| + \frac{b}{l})\chi_{\tilde{\sigma}(t_k)} \right), \quad (82)$$

$$\chi_{\tilde{\sigma}(t_k)} \triangleq \|H_{\tilde{\sigma}(t_k)}(s)(I - BT(s))\|_{\mathcal{L}_1} l. \quad (83)$$

With these definitions at hand, we now present the performance of RHAC in the following theorem, whose proof appears in Appendix F.

Theorem 5: Consider the real vehicle dynamics (31) controlled by the \mathcal{L}_1 -based RHAC comprised of (72), (73), (77), (80) and (80), after $t = t_{k^*}$. If the minimum dwell time satisfies (64) for reference (10) and satisfies (66) for reference (11), $e(t_{k^*}) \in \Theta_{\sigma(t_{k^*})}$, $\varepsilon > 0$, and

$$\varepsilon + \delta \leq \frac{1}{\sqrt{\lambda_{\max}(P_{\sigma(t_k)})}}, \quad (84)$$

then $e(t) \in \Phi_{\sigma(t_k)}$ and $\|x(t) - \bar{x}(t)\| \leq \varepsilon$, for any $t \in [t_k, t_{k+1})$, $k \geq k^* \in \mathbb{N}$.

Remark 16: When physical or software failures or unforeseen environment influence lead to the triggering conditions in the switching **Rule I** and/or **II**, RHAC will be activated to prevent the state from further divergence. According to Theorem 5, at the switching moment if the tracking error is inside the safety envelope, the real state $x(t)$ follows the state $\bar{x}(t)$ of the vehicle model reference with a bias ε . Therefore, $x(t)$ always remains inside Ω by Lemma 2. As a consequence, in light of Lemma 1, the real state $x(t)$ never violates the safety constraint (14).

VII. SIMULATION

This section focuses on demonstration of safe autonomous velocity regulation via RHAC in dynamic normal driving environments and an unforeseen environment. Following real examples in [6], [11], [34], [37], the vehicle parameter values used for simulation are given in Table II.

Table II
VEHICLE PARAMETER VALUES

m	J	r	ζ	q	C	r_b	η_b	l_r	l
540kg	5kg-m ²	0.31m	25Ns/m ²	1Nms/rad	11.34cm ²	124mm	0.38	1.14m	2.63m

A. Dynamic Normal Driving Environments

We assume the vehicle continuously drives between normal snow and icy roads. Therefore, in the dynamic environments we have

$$\mathbb{S}/\{\text{hpc, learned}\} = \{\text{snow}^1, \text{snow}^2, \text{icy}^1, \text{icy}^2\}.$$

For the road friction models, we let $k_{\text{snow}} = 70\text{Nms/rad}$ and $k_{\text{icy}} = 35\text{Nms/rad}$. For the angular references, we choose $w_{\text{snow}}^* = 40\text{rad/s}$ and $w_{\text{icy}}^* = 20\text{rad/s}$. The longitudinal velocity references are computed via (12). For the state bias, we let $\varepsilon = 1.5$. We set the slip safety boundaries as $\mu_{\text{snow}} = \mu_{\text{icy}} = 1\text{m/s}$. We let minimum dwell time on each road be $\text{dwell}_{\text{min}} = 30\text{sec}$. By (19), we have

$$\hat{c}_{\text{snow}^1} = [-0.5543, 1.7880]^\top, \quad \hat{c}_{\text{snow}^2} = [-0.5267, 1.6991]^\top, \\ \hat{c}_{\text{icy}^1} = [-0.5709, 0.6481]^\top, \quad \hat{c}_{\text{icy}^2} = [-0.5152, 0.6243]^\top.$$

Then, by the formulae (59) and (60), the switching controller matrices are solved by LMI toolbox as

$$F_{\text{snow}^1} = \begin{bmatrix} 41.70 & -128.6 \\ -60.70 & 190.60 \end{bmatrix}, \quad F_{\text{snow}^2} = \begin{bmatrix} -14.40 & 23.20 \\ 25.30 & -58.20 \end{bmatrix}, \\ F_{\text{icy}^1} = \begin{bmatrix} 583.20 & -1953.6 \\ 596.0 & 1995.1 \end{bmatrix}, \quad F_{\text{icy}^2} = \begin{bmatrix} -52.10 & 164.9 \\ 54.30 & -172.2 \end{bmatrix}.$$

For the uncertainties in (3), we set

$$\tilde{f}_w(t) = \begin{cases} 0.01v^2(t) + 0.5 \cos(t), & \text{snow road} \\ 0.05v(t) + 0.1 \cos(v(t)), & \text{icy road} \end{cases} \\ \tilde{f}_v(t) = \begin{cases} 0.05 \sin(5w(t)) \sin(t), & \text{snow road} \\ 0.5 \sin(v(t)) \sin(t), & \text{icy road.} \end{cases}$$

In the simulation, we let the vehicle periodically drive in two roads. The dwell times on the snow and icy roads are respectively set as $\text{dwell}_{\text{snow}} = 120\text{sec}$ and $\text{dwell}_{\text{icy}} = 150\text{sec}$. With $x(0) = [50\text{rad/s}, 16\text{m/s}]^\top$, the trajectory of velocities and slip are shown in Figure 7, from which we observe that the developed \mathcal{L}_1 -based RHAC succeeds in safe autonomous velocity regulation in the dynamic adverse driving environments.

B. Unforeseen Driving Environment

In the unforeseen driving environment, we assume that all the environment relations and characteristics, e.g., viscous torque (1), longitudinal aerodynamic drag force (2) and traction torque are unknown. In simulations, we set the previous normal environmental parameter as $k_{\text{icy}} = 20\text{Nms/rad}$, and the uncertainties

$$\tilde{f}_w(t) = 0.005v^2(t) + 0.5 \cos(5t), \quad \tilde{f}_v(t) = 0.05 \sin(v(t)) \sin(t),$$

others are the same as those in previous subsection. We let the vehicle enter the unforeseen environment at $t = 120\text{sec}$, and we then change the uncertainties to

$$\tilde{f}_w(t) = -0.3v^2(t) + 3 \cos(5t), \quad \tilde{f}_v(t) = 3 \sin(v(t)) \sin(t).$$

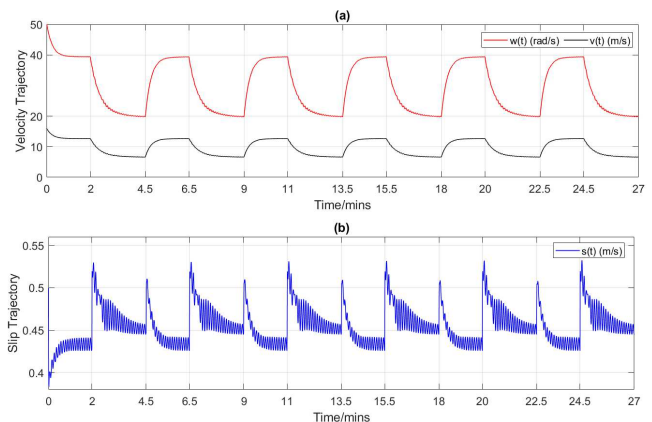


Figure 7. Vehicle and slip trajectories: velocities track the given references, slips are constrained below the preset safety boundaries $\mu_{\text{snow}} = \mu_{\text{icy}} = 1\text{m/s}$.

For model learning, we set the sampling period $T = 0.0091\text{sec}$ and recorded data length $\kappa = 0.1\text{sec}$. For slip, we set its safety boundary $\mu_{\text{icy}} = \mu_{\text{learned}} = 3\text{m/s}$. For its safety envelop defined in (26), we set $\theta = 0.35$. As shown in Figure 8 (a), the learned model is activated at $t = 121\text{sec}$ via real-time verification of safety envelope. The learned system matrix is

$$A_{\text{learned}} = \begin{bmatrix} 4.3189 & -14.7060 \\ -0.1436 & 0.3929 \end{bmatrix}.$$

The control matrix is then updated as

$$F_{\text{learned}} = \begin{bmatrix} -58.9488 & 249.9351 \\ 52.8046 & -226.7951 \end{bmatrix}.$$

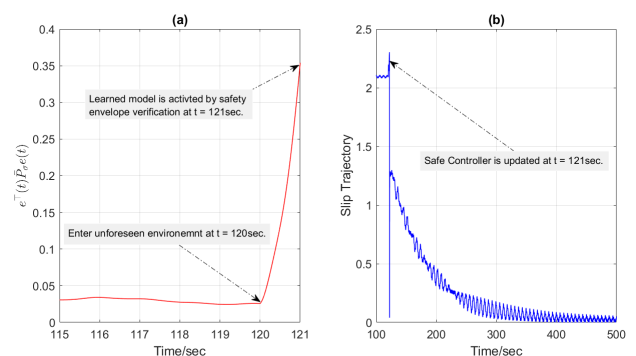


Figure 8. (a) Learned model is activated at $t = 121\text{sec}$ by safety envelope verification, (2) after the safe controller updated, wheel slip is constrained to safe set.

The trajectory of slip in Figure 8 (b) and the trajectories of velocities in Figure 9 show that using the learned vehicle model reference (40), RHAC succeeds in regulating the velocities to zeros while restricting the wheel slip to the safety set in the unforeseen environment.

VIII. CONCLUSION

In this paper, we have proposed a model-learning based \mathcal{L}_1 -Simplex architecture for safe autonomous velocity regulation

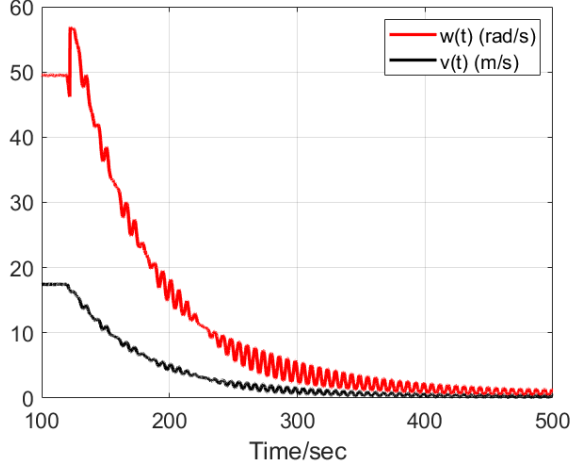


Figure 9. Vehicle velocity trajectories: after learned vehicle model is activated at $t = 121\text{sec}$, velocities track the given references.

through integration of TCS and ABS. To make the \mathcal{L}_1 -Simplex more reliable, finite-time model learning is incorporated into \mathcal{L}_1 -based verified safe control, where the short-term state data from a single trajectory generated in the unprepared or unforeseen environments are used to adaptively update vehicle model for reliable control actuation computation. Simulations demonstrate the effectiveness of the \mathcal{L}_1 -Simplex for longitudinal vehicle control systems.

Exploring the model-learning based \mathcal{L}_1 -Simplex in coordinating lateral motion control and longitudinal motion control of autonomous vehicles, as well as the demonstrations in full-size car, constitute our future research direction.

APPENDIX A: PROOF OF LEMMA 1

Substituting (19) into (20) yields $-1 \leq \frac{e_v}{\mu_\sigma - \frac{\zeta r^2 \mathbf{v}_\sigma^r}{k_\sigma}} - \frac{r e_w}{\mu_\sigma - \frac{\zeta r^2 \mathbf{v}_\sigma^r}{k_\sigma}} \leq 1$, which, in conjunction with the relation $\mu_\sigma \geq \frac{\zeta r^2 \mathbf{v}_\sigma^r}{k_\sigma}$ (indicated by (17)), leads to

$$-\mu_\sigma + \frac{\zeta r^2 \mathbf{v}_\sigma^r}{k_\sigma} \leq e_v - r e_w \leq \mu_\sigma - \frac{\zeta r^2 \mathbf{v}_\sigma^r}{k_\sigma}. \quad (85)$$

It straightforwardly follows from $\mu_\sigma - \frac{\zeta r^2 \mathbf{v}_\sigma^r}{k_\sigma} \leq \mu_\sigma + \frac{\zeta r^2 \mathbf{v}_\sigma^r}{k_\sigma}$ that (85) implies (17) and (18). Moreover, (17) and (18) equivalently describe the safety condition (14) via the transformations (15) and (16). Thus, (14) holds if (20) is satisfied.

APPENDIX B: PROOF OF THEOREM 2

For simplicity, let us denote

$$a_{11} \triangleq \frac{k_\sigma}{J} - \frac{g}{J} - F_{\sigma^1}^w, \quad a_{12} \triangleq \frac{k_\sigma}{rJ} + F_{\sigma^1}^v, \quad a_{21} = \frac{k_\sigma}{mr}, \quad (86a)$$

$$a_{22} \triangleq \frac{k_\sigma - \zeta r^2}{mr^2}, \quad b_{11} = -\frac{k_\sigma}{J} - \frac{g}{J} - F_{\sigma^2}^w, \quad (86b)$$

$$b_{12} \triangleq \frac{k_\sigma}{rJ} - F_{\sigma^2}^v, \quad b_{22} = \frac{-k_\sigma - \zeta r^2}{mr^2}. \quad (86c)$$

It is straightforward to verify from (51) and (52) that $\det(\lambda I - \hat{A}_{\sigma^1}) = 0$ and $\det(\lambda I - \hat{A}_{\sigma^2}) = 0$ respectively

equate to $\lambda^2 - \lambda(a_{11} + a_{22}) + a_{11}a_{22} - a_{12}a_{21} = 0$ and $\lambda^2 - \lambda(b_{22} + b_{11}) + b_{22}b_{11} - a_{21}b_{12} = 0$, which further implies that \hat{A}_{σ^1} and \hat{A}_{σ^2} are Hurwitz if and only if

$$a_{11} + a_{22} < 0, \quad a_{11}a_{22} - a_{12}a_{21} > 0, \quad (87)$$

$$b_{11} + b_{22} < 0, \quad b_{22}b_{11} - a_{21}b_{12} > 0. \quad (88)$$

For \hat{A}_{σ^1} , substituting the definitions of a_{11} , a_{12} , a_{21} and a_{22} into (87) equivalently leads to (54). For \hat{A}_{σ^2} , substituting the definitions of b_{11} , a_{21} , b_{12} and b_{22} into (88) equivalently leads to (55).

APPENDIX C: PROOF OF LEMMA 3

In light of the definitions given in (86), the system matrices (51) and (52) are rewritten as

$$\hat{A}_{\sigma^1} = \begin{bmatrix} -a_{11} & -a_{12} \\ -a_{21} & a_{22} \end{bmatrix}, \quad \hat{A}_{\sigma^2} = \begin{bmatrix} b_{11} & b_{12} \\ a_{21} & b_{22} \end{bmatrix}. \quad (89)$$

To finish the proof, we only need to prove that there exist feasible control gains $F_{\sigma^1}^w$, $F_{\sigma^2}^w$, $F_{\sigma^1}^v$, $F_{\sigma^2}^v$, and $\bar{P}_\sigma > 0$ such that (56) holds. Let us choose $\bar{P}_\sigma = \begin{bmatrix} p_1^\sigma & -1 \\ -1 & p_2^\sigma \end{bmatrix} > 0$, by which (56) and (89) lead

$$\begin{aligned} & \hat{A}_{\sigma^1}^\top \bar{P}_\sigma + \bar{P}_\sigma \hat{A}_{\sigma^1} \\ &= \begin{bmatrix} 2a_{11}p_1^\sigma + 2a_{21} & -a_{22} - a_{11} - a_{21}p_2^\sigma - a_{12}p_1^\sigma \\ * & 2a_{22}p_2^\sigma + 2a_{12} \end{bmatrix}, \\ & \hat{A}_{\sigma^2}^\top \bar{P}_\sigma + \bar{P}_\sigma \hat{A}_{\sigma^2} \\ &= \begin{bmatrix} 2b_{11}p_1^\sigma - 2a_{21} & -b_{11} - b_{22} + a_{21}p_2^\sigma + b_{12}p_1^\sigma \\ * & -2b_{12} + 2b_{22}p_2^\sigma \end{bmatrix}, \end{aligned}$$

which, in conjunction with (86), leads to

$$(A_{\sigma^1}^\top \bar{P}_\sigma + \bar{P}_\sigma A_{\sigma^1}) - (A_{\sigma^2}^\top \bar{P}_\sigma + \bar{P}_\sigma A_{\sigma^2}) = \begin{bmatrix} k_1 & k_2 \\ k_2 & k_3 \end{bmatrix}, \quad (90)$$

where

$$k_1 \triangleq \frac{4k_\sigma p_1^\sigma}{J} + \frac{4k_\sigma}{mr} + 2(F_{\sigma^2}^w - F_{\sigma^1}^w)p_1^\sigma,$$

$$k_3 \triangleq \frac{4k_\sigma p_2^\sigma}{mr^2} + \frac{4k_\sigma}{rJ} + 2(F_{\sigma^1}^v - F_{\sigma^2}^v),$$

$$k_2 \triangleq -\frac{2(1+rp_2^\sigma)k_\sigma}{mr^2} - \frac{2(r+p_1^\sigma)k_\sigma}{rJ} + (F_{\sigma^2}^v - F_{\sigma^1}^v)p_1^\sigma + F_{\sigma^1}^w - F_{\sigma^2}^w.$$

Meanwhile, if $k_2 \leq 0$ and $F_{\sigma^2}^w = F_{\sigma^1}^w$, we have

$$k_1 - |k_2| = \frac{4k_\sigma p_1^\sigma}{J} + \frac{4k_\sigma}{mr} - \frac{2(1+rp_2^\sigma)k_\sigma}{mr^2} - \frac{2(r+p_1^\sigma)k_\sigma}{rJ} + (F_{\sigma^2}^v - F_{\sigma^1}^v)p_1^\sigma, \quad (91)$$

$$k_3 - |k_2| = \frac{4k_\sigma p_2^\sigma}{mr^2} - \frac{2(1+rp_2^\sigma)k_\sigma}{mr^2} + \frac{4k_\sigma}{rJ} - \frac{2(r+p_1^\sigma)k_\sigma}{rJ} + (F_{\sigma^2}^v - F_{\sigma^1}^v)(p_1^\sigma - 2). \quad (92)$$

With the consideration of (54) and (55), we can let $F_{\sigma^2}^w = F_{\sigma^1}^w$, and choose a $p_2^\sigma > 0$ such that $k_1 > 0$, $k_3 > 0$ and $k_2 \leq 0$. The second items in (54) and (55) imply that if $F_{\sigma^2}^w = F_{\sigma^1}^w$, we can have $F_{\sigma^2}^v - F_{\sigma^1}^v > 0$, which, in conjunction with (91) and (92), indicate that given a fixed $p_1^\sigma > 2$, through adjustment of the magnitude of $F_{\sigma^2}^v - F_{\sigma^1}^v$, we have $k_1 > |k_2|$ and $k_3 > |k_2|$. Therefore, we conclude from (90) that $\hat{A}_{\sigma^1}^\top \bar{P}_\sigma + \bar{P}_\sigma \hat{A}_{\sigma^1} > \hat{A}_{\sigma^2}^\top \bar{P}_\sigma + \bar{P}_\sigma \hat{A}_{\sigma^2}$. Under

(54), \widehat{A}_{σ^1} is Hurwitz, such that we can choose a $\bar{P}_\sigma > 0$ that $\widehat{A}_{\sigma^1}^\top \bar{P}_\sigma + \bar{P}_\sigma \widehat{A}_{\sigma^1} < 0$. As a consequence, we have $\widehat{A}_{\sigma^2}^\top \bar{P}_\sigma + \bar{P}_\sigma \widehat{A}_{\sigma^2} < 0$.

To finish the proof, we should also consider \bar{P}_σ in the form $\bar{P}_\sigma = \begin{bmatrix} p_1^\sigma & 1 \\ 1 & p_2^\sigma \end{bmatrix}$. Following the same steps above, we get the same conclusion (56).

APPENDIX D: PROOF OF THEOREM 3

The formula (59) equivalently transforms to

$$\bar{P}_\sigma > 0, \quad \forall \sigma \in \mathbb{U} \quad (93a)$$

$$\hat{c}_\sigma^\top \bar{P}_\sigma^{-1} \hat{c}_\sigma \leq 1, \quad \forall \sigma \in \mathbb{U} \quad (93b)$$

$$\bar{P}_\sigma \bar{A}_{\sigma^i} + \bar{A}_{\sigma^i}^\top \bar{P}_\sigma < 0, \quad \forall \sigma \in \mathbb{S}, i = 1, 2 \quad (93c)$$

$$\bar{P}_{\text{learned}} \bar{A}_{\text{learned}} + \bar{A}_{\text{learned}}^\top \bar{P}_{\text{learned}} < 0, \quad (93d)$$

where \bar{A}_{σ^i} and \bar{A}_{learned} are given in (61). We now consider the function:

$$V_{\sigma(\bar{t}_k)}(\bar{e}(t)) = \bar{e}^\top(t) \bar{P}_{\sigma(\bar{t}_k)} \bar{e}(t), t \in [\bar{t}_k, \bar{t}_{k+1}), \quad (94)$$

where \bar{t}_k denotes the switching times.

Following the proof of Theorem 3.1 in [38] we conclude that if the conditions (93a), (93c), (93d) and (64) hold, we have

$$\dot{V}_{\sigma(\bar{t}_k)}(\bar{e}(t)) < 0, \quad t \in [\bar{t}_k, \bar{t}_{k+1}), \quad (95)$$

$$V_{\sigma(\bar{t}_k)}(\bar{e}(\bar{t}_{k+1})) \leq \phi V_{\sigma(\bar{t}_{k-1})}(\bar{e}(\bar{t}_k)), \quad \forall k \in \mathbb{N}, \quad (96)$$

where

$$0 < \phi = \max_{p \neq q \in \mathbb{U}} \{e^{\text{dwell}_{\min} \lambda_{\max}^p \lambda_{\min}^{-1}(P_p)} \lambda_{\max}(P_p) \lambda_{\min}^{-1}(P_q)\} < 1.$$

We note that (95) and (96) indicate that $V_{\sigma(\bar{t}_k)}(\bar{e}(t)) < V_{\sigma(\bar{t}_0)}(\bar{e}(t_0))$ for any $t > t_0$ and $\forall k \in \mathbb{N}$. Therefore, we conclude that if $\bar{e}(t_0) \in \Theta_{\sigma(t_0)}$, $\bar{e}(t) \in \Theta_{\sigma(\bar{t}_0)}$ for any $t \geq t_0$. As a consequence, $\bar{e}(t) \in \Theta = \bigcup_{\sigma \in \mathbb{U}} \Theta_\sigma$ for any $t \geq t_0$.

With the consideration of (95) and (96), we can construct a strictly decreasing sequence with respect to k : $\{V_{\sigma(\bar{t}_k)}(\bar{e}(t_k)), k \in \mathbb{N}\}$. The decreasing sequence straightforwardly implies that the switched linear system is asymptotically stable.

APPENDIX E: PROOF OF THEOREM 4

Following the proof of Theorem 3, we also let \bar{t}_k denote the switching time. The function (94) can still be used for the dynamics (65). Noticing (93c) and definitions (62) and (63), its time derivative satisfies

$$\begin{aligned} \dot{V}_{\sigma(\bar{t}_k)}(\bar{e}(t)) &\leq \lambda_{\max}^{\sigma(\bar{t}_k)} \bar{e}^\top(t) e(t) \\ &= \lambda_{\max}^{\sigma(\bar{t}_k)} \lambda_{\max}^{-1}(\bar{P}_{\sigma(\bar{t}_k)}) \lambda_{\max}(\bar{P}_{\sigma(\bar{t}_k)}) \bar{e}^\top(t) \bar{e}(t) \\ &\leq \lambda_{\max}^{\sigma(\bar{t}_k)} \lambda_{\max}^{-1}(\bar{P}_{\sigma(\bar{t}_k)}) V_{\sigma(\bar{t}_k)}(\bar{e}(t)) < 0, \end{aligned} \quad (97)$$

where the inequality (97) from previous step is obtained via considering the fact $\lambda_{\max}^{\sigma(\bar{t}_k)} < 0$.

It follows from (94), (65) and (97) that

$$\begin{aligned} &V_{\sigma(\bar{t}_k)}(\bar{e}(t_k)) \\ &= \bar{e}^\top(\bar{t}_k^-) (E_k^\top \bar{P}_{\sigma(\bar{t}_k)} E_k) \bar{e}(\bar{t}_k^-) \\ &\leq \lambda_{\max}(E_k^\top \bar{P}_{\sigma(\bar{t}_k)} E_k) \bar{e}^\top(\bar{t}_k^-) \bar{e}(\bar{t}_k^-) \\ &\leq \frac{\lambda_{\max}(E_k^\top \bar{P}_{\sigma(\bar{t}_k)} E_k)}{\lambda_{\min}(\bar{P}_{\sigma(\bar{t}_{k-1})})} V_{\sigma(\bar{t}_{k-1})}(\bar{e}(\bar{t}_k^-)) \\ &\leq \frac{\lambda_{\max}(E_k^\top \bar{P}_{\sigma(\bar{t}_k)} E_k)}{\lambda_{\min}(\bar{P}_{\sigma(\bar{t}_{k-1})})} e^{\frac{\lambda_{\max}^{\sigma(\bar{t}_{k-1})}(\bar{t}_k - \bar{t}_{k-1})}{\lambda_{\max}(P_{\sigma(\bar{t}_{k-1})})}} V_{\sigma(\bar{t}_{k-1})}(\bar{e}(\bar{t}_{k-1})) \\ &\leq \nu_k V_{\sigma(\bar{t}_{k-1})}(\bar{e}(\bar{t}_{k-1})), \end{aligned} \quad (98)$$

where $\nu_k = \frac{\lambda_{\max}(E_k^\top \bar{P}_{\sigma(\bar{t}_k)} E_k)}{\lambda_{\min}(P_{\sigma(\bar{t}_{k-1})})} e^{\frac{\lambda_{\max}^{\sigma(\bar{t}_{k-1})} \text{dwell}_{\min}}{\lambda_{\max}(P_{\sigma(\bar{t}_{k-1})})}}$. We note that the third inequality therein is obtained via the integration of (97), while (98) from previous step is obtained via considering $\lambda_{\max}^{\sigma(\bar{t}_{k-1})} < 0$ implied by (93c) and (93d).

The condition of dwell_{\min} in Theorem 4 implies $0 < \nu \triangleq \min_{k \in \mathbb{N}} \{\nu_k\} < 1$ for $\forall k \in \mathbb{N}$. Thus, we have

$$V_{\sigma(\bar{t}_k)}(\bar{e}(\bar{t}_k)) < \nu V_{\sigma(\bar{t}_{k-1})}(\bar{e}(\bar{t}_{k-1})), \quad (99)$$

by which we can construct a strictly decreasing sequence with respect to k : $\{V_{\sigma(\bar{t}_k)}(\bar{e}(t_k)), k \in \mathbb{N}\}$. The decreasing sequence straightforwardly implies that the switched system (57) is asymptotically stable.

We note that (95) still holds for this impulsive switched system, thus, $V_{\sigma(\bar{t}_k)}(\bar{e}(\bar{t}_k)) < V_{\sigma(\bar{t}_k)}(\bar{e}(t))$ for any $t > \bar{t}_k$. We obtain $V_{\sigma(\bar{t}_k)}(\bar{e}(t)) < V_{\sigma(\bar{t}_0)}(\bar{e}(t_0))$ for any $t > t_0$ and $\forall k \in \mathbb{N}$. Therefore, we conclude that if $\bar{e}(t_0) \in \Theta_{\sigma(t_0)}$, $\bar{e}(t) \in \Theta_{\sigma(\bar{t}_0)}$ for any $t \geq t_0$. As a consequence, $x(t) \in \Theta = \bigcup_{\sigma \in \mathbb{U}} \Theta_\sigma$ for any $t \geq t_0$.

APPENDIX F: PROOF OF THEOREM 5

The proof follows the same procedure of Theorem 4.10 of [25]. We thus only present the critical differences:

$$\begin{aligned} &\|x(s) - \bar{x}(s)\|_{\mathcal{L}_\infty[t_k, t_{k+1})} \\ &\leq \|H_{\bar{\sigma}(t_k)}(s) B T(s)(s + \alpha)\|_{\mathcal{L}_1} \sqrt{\frac{\mu}{K}} + M_{\bar{\sigma}(t_k)}, \end{aligned} \quad (100)$$

where

$$\mu \triangleq 4\rho^2 + \frac{4\alpha\rho^2 + 2\rho l}{\alpha} \left(\frac{1}{1 - e^{-2\alpha \text{dwell}_{\min}}} + 1 \right), \quad (101)$$

$$M_{\bar{\sigma}(t_k)} \triangleq \|H_{\bar{\sigma}(t_k)}(s)(\mathbf{I} - B T(s))\|_{\mathcal{L}_1} \left\| \check{f}(t)(s) \right\|_{\mathcal{L}_\infty[t_k, t_{k+1})}. \quad (102)$$

For the considered velocity reference (11), (10) and (49), further following (95) and (96) yields the same result as

$$\begin{aligned} \bar{e}^\top(t) P_{\sigma(\bar{t}_k)} \bar{e}(t) &= V_{\sigma(\bar{t}_k)}(\bar{e}(t)) < V_{\sigma(t_{k^*})}(\bar{e}(t_{k^*})) \\ &= \bar{e}^\top(t_{k^*}) P_{\sigma(t_{k^*})} \bar{e}(t_{k^*}), \end{aligned} \quad (103)$$

for any $t \in [\bar{t}_k, \bar{t}_{k+1})$ with $\bar{t}_k \geq t_{k^*}$, $\forall k \in \mathbb{N}$.

With the consideration of δ given by (81), the inequality (103) implies

$$\|\bar{e}\|_{\mathcal{L}_\infty[t_k, t_{k+1}]} < \delta, \quad k \geq k^* \in \mathbb{N}. \quad (104)$$

It follows from (68) that

$$\left\| \check{f}_q(s) \right\|_{\mathcal{L}_\infty[t_k, t_{k+1}]} \leq l \|x(s)\|_{\mathcal{L}_\infty[t_k, t_{k+1}]} + b, \quad q = 0, 1 \quad (105)$$

where l and b are given in (75).

Combining (102) with (104) and (105) yields

$$\begin{aligned} & M_{\bar{\sigma}(t_k)} \\ & \leq \left\| H_{\bar{\sigma}(t_k)}(s)(I - BT(s)) \right\|_{\mathcal{L}_1} (l \|x(s)\|_{\mathcal{L}_\infty[t_k, t_{k+1}]} + b) \\ & = \chi_{\bar{\sigma}(t_k)} (\|x(s)\|_{\mathcal{L}_\infty[t_k, t_{k+1}]} + \frac{b}{l}) \\ & \leq \chi_{\bar{\sigma}(t_k)} (\|x - \bar{x}\|_{\mathcal{L}_\infty[t_k, t_{k+1}]} + \|\bar{x}\|_{\mathcal{L}_\infty[t_k, t_{k+1}]} + \frac{b}{l}) \\ & \leq \chi_{\bar{\sigma}(t_k)} (\|x - \bar{x}\|_{\mathcal{L}_\infty[t_k, t_{k+1}]} + \|\bar{e}\|_{\mathcal{L}_\infty[t_k, t_{k+1}]} + \|x_{\bar{\sigma}(t_k)}^*\|) + \frac{b}{l}, \\ & < \chi_{\bar{\sigma}(t_k)} (\|x - \bar{x}\|_{\mathcal{L}_\infty[t_k, t_{k+1}]} + \delta + \|x_{\bar{\sigma}(t_k)}^*\|) + \frac{b}{l}, \end{aligned} \quad (106)$$

where $\chi_{\bar{\sigma}(t_k)}$ is given by (83).

Substituting (106) into (100) yields

$$\begin{aligned} & (1 - \chi_{\bar{\sigma}(t_k)}) \|x(s) - \bar{x}(s)\|_{\mathcal{L}_\infty[t_k, t_{k+1}]} \\ & < \left\| H_{\bar{\sigma}(t_k)}(s)BT(s)(s + \alpha) \right\|_{\mathcal{L}_1} \sqrt{\frac{\mu}{K}} + \chi_{\bar{\sigma}(t_k)} (\delta + \|x_{\bar{\sigma}(t_k)}^*\|) + \frac{b}{l}, \end{aligned}$$

which, in conjunction with $\varepsilon > 0$ (given in (82)), results in $\|x(t) - \bar{x}(t)\| \leq \varepsilon$.

REFERENCES

- [1] G. Dimitrakopoulos and P. Demestichas, "Intelligent transportation systems," *IEEE Vehicular Technology Magazine*, vol. 5, no. 1, pp. 77–84, 2010.
- [2] V. Ivanov, D. Savitski, and B. Shyrokau, "A survey of traction control and antilock braking systems of full electric vehicles with individually controlled electric motors," *IEEE Transactions on Vehicular Technology*, vol. 64, no. 9, pp. 3878–3896, 2014.
- [3] S. M. Savaresi and M. Tanelli, *Active braking control systems design for vehicles*. Springer Science & Business Media, 2010.
- [4] A. A. Aly, E.-S. Zeidan, A. Hamed, F. Salem *et al.*, "An antilock-braking systems (ABS) control: A technical review," *Intelligent Control and Automation*, vol. 2, no. 03, pp. 186–195, 2011.
- [5] K. Reif, "Brakes, brake control and driver assistance systems," *Weisbaden, Germany, Springer Vieweg*, 2014.
- [6] F. Borrelli, A. Bemporad, M. Fodor, and D. Hrovat, "An MPC/hybrid system approach to traction control," *IEEE Transactions on Control Systems Technology*, vol. 14, no. 3, pp. 541–552, 2006.
- [7] C. C. De Wit and P. Tsiotras, "Dynamic tire friction models for vehicle traction control," in *Proceedings of the 38th IEEE Conference on Decision and Control*, pp. 3746–3751, 1999.
- [8] V. Colli, G. Tomassi, and M. Scarano, "Single wheel longitudinal traction control for electric vehicles," *IEEE Transactions on Power Electronics*, vol. 21, no. 3, pp. 799–808, 2006.
- [9] E. Reichensdörfer, D. Odenthal, and D. Wollherr, "On the stability of nonlinear wheel-slip zero dynamics in traction control systems," *IEEE Transactions on Control Systems Technology*, 2018.
- [10] D. Yin, S. Oh, and Y. Hori, "A novel traction control for EV based on maximum transmissible torque estimation," *IEEE Transactions on Industrial Electronics*, vol. 56, no. 6, pp. 2086–2094, 2009.
- [11] K. Han, S. B. Choi, J. Lee, D. Hyun, and J. Lee, "Accurate brake torque estimation with adaptive uncertainty compensation using a brake force distribution characteristic," *IEEE Transactions on Vehicular Technology*, vol. 66, no. 12, pp. 10 830–10 840, 2017.
- [12] G. A. Magallan, C. H. De Angelo, and G. O. Garcia, "Maximization of the traction forces in a 2WD electric vehicle," *IEEE Transactions on Vehicular Technology*, vol. 60, no. 2, pp. 369–380, 2010.
- [13] P. Khatun, C. M. Bingham, N. Schofield, and P. Mellor, "Application of fuzzy control algorithms for electric vehicle antilock braking/traction control systems," *IEEE Transactions on Vehicular Technology*, vol. 52, no. 5, pp. 1356–1364, 2003.
- [14] K. Han, M. Choi, B. Lee, and S. B. Choi, "Development of a traction control system using a special type of sliding mode controller for hybrid 4wd vehicles," *IEEE transactions on vehicular technology*, vol. 67, no. 1, pp. 264–274, 2017.
- [15] S. De Pinto, C. Chatzikomis, A. Sornioti, and G. Mantriota, "Comparison of traction controllers for electric vehicles with on-board drive-trains," *IEEE Transactions on Vehicular Technology*, vol. 66, no. 8, pp. 6715–6727, 2017.
- [16] J. E. A. Dias, G. A. S. Pereira, and R. M. Palhares, "Longitudinal model identification and velocity control of an autonomous car," *IEEE Transactions on Intelligent Transportation Systems*, vol. 16, no. 2, pp. 776–786, 2014.
- [17] X. Sun, Y. Cai, S. Wang, X. Xu, and L. Chen, "Optimal control of intelligent vehicle longitudinal dynamics via hybrid model predictive control," *Robotics and Autonomous Systems*, vol. 112, pp. 190–200, 2019.
- [18] M. Tai and M. Tomizuka, "Robust longitudinal velocity tracking of vehicles using traction and brake control," in *6th International Workshop on Advanced Motion Control. Proceedings*, pp. 305–310, 2000.
- [19] L. Sha, "Using simplicity to control complexity," *IEEE Software*, no. 4, pp. 20–28, 2001.
- [20] N. Hovakimyan and C. Cao, *L1 Adaptive Control Theory: Guaranteed Robustness with Fast Adaptation*. SIAM, 2010.
- [21] N. Hovakimyan, C. Cao, E. Kharisov, E. Xargay, and I. M. Gregory, "L1 adaptive control for safety-critical systems," *IEEE Control Systems Magazine*, 2011.
- [22] K. Ackerman, E. Xargay, R. Choe, N. Hovakimyan, M. C. Cotting, R. B. Jeffrey, M. P. Blackstun, T. P. Fulkerson, T. R. Lau, and S. S. Stephens, "L1 stability augmentation system for Calspan's variable-stability Learjet," in *AIAA Guidance, Navigation, and Control Conference*, pp. 0631, 2016.
- [23] T. Leman, E. Xargay, G. Dullerud, N. Hovakimyan, and T. Wendel, "L1 adaptive control augmentation system for the X-48B aircraft," in *AIAA guidance, navigation, and control conference*, pp. 5619, 2009.
- [24] R. Choe, O. Stroosma, E. Xargay, H. Damveld, N. Hovakimyan, J. Mulder, and H. Damveld, "A handling qualities assessment of a business jet augmented with an L1 adaptive controller," in *AIAA guidance, navigation, and control conference*, pp. 6610, 2011.
- [25] X. Wang, N. Hovakimyan, and L. Sha, "RSimplex: A robust control architecture for cyber and physical failures," *ACM Transactions on Cyber-Physical Systems*, vol. 2, no. 4, 2018.
- [26] R. Rajamani, *Vehicle dynamics and control*. Springer Science & Business Media, 2011.
- [27] L. Asmelash, "Everything you need to know about snow squalls," <https://www.cnn.com/2019/12/19/weather/snow-squall-what-is-explain-trnd/index.html> accessed 2020-07-27.
- [28] Y. Jedra and A. Proutiere, "Finite-time identification of stable linear systems: Optimality of the Least-Squares estimator," *arXiv:2003.07937*, 2020.
- [29] T. Sarkar and A. Rakhlin, "Near optimal finite time identification of arbitrary linear dynamical systems," in *International Conference on Machine Learning*, pp. 5610–5618, 2019.
- [30] T. Sarkar, A. Rakhlin, and M. A. Dahleh, "Finite-time system identification for partially observed LTI systems of unknown order," *arXiv:1902.01848*, 2019.
- [31] M. Simchowitz, H. Mania, S. Tu, M. I. Jordan, and B. Recht, "Learning without mixing: Towards a sharp analysis of linear system identification," in *Conference On Learning Theory*, pp. 1–35, 2018.
- [32] D. J. Foster, A. Rakhlin, and T. Sarkar, "Learning nonlinear dynamical systems from a single trajectory," *arXiv:2004.14681*, 2020.
- [33] Y. Mao, N. Hovakimyan, P. Voulgaris, and L. Sha, "Finite-time model inference from a single system trajectory," https://www.dropbox.com/s/v06asvinhig6zzf/Fast_Model_Learning.pdf?dl=0.
- [34] W. Kirchner and S. C. Southward, "An anthropomorphic approach to high performance traction control," *Paladyn, Journal of Behavioral Robotics*, vol. 2, no. 1, pp. 25–35, 2011.
- [35] D. Seto and L. Sha, "An engineering method for safety region development," *CMU/SEI-99-TR-018*, 1999.
- [36] D. Liberzon, *Switching in systems and control*. Springer Science & Business Media, 2003.

- [37] K. Han, B. Lee, and S. B. Choi, "Development of an antilock brake system for electric vehicles without wheel slip and road friction information," *IEEE Transactions on Vehicular Technology*, vol. 68, no. 6, pp. 5506–5517, 2019.
- [38] W. Ni, D. Cheng, and X. Hu, "Minimum dwell time for stability and stabilization of switched linear systems," in *2008 7th World Congress on Intelligent Control and Automation*, pp. 4109–4115, 2008.